ENTRAINMENT IN SALDANHA BAY

B Spolander

Thesis submitted to the University of Cape Town in fulfillment
of the requirements of the degree of Master of Science

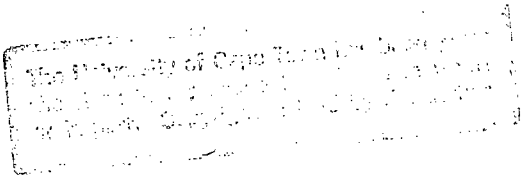

Contents

List of Figures

Chapter 1

INTRODUCTION

Saldanha Bay is located $100km$ north of Cape Town, along the south western coast of South Africa, at a latitude of approximately $33°S$. In 1975 major harbour works, including the construction of an iron ore jetty, divided Saldanha Bay into two distinct bays. The bay to the north of the jetty has become known as Small Bay, while the bay to the south is commonly referred to as Big Bay. Big Bay is connected at its southern end to the shallow Langebaan Lagoon system, and to the west with the Benguela upwelling system (see figure 1.1).

The oceanography of the shelf outside the bay is dominated by the coastal upwelling system (Shannon 1985). The equatorward winds which predominate for much of the year, drive an offshore flux of surface water, which is replaced near the coast by nutrient-rich water from deeper layers. These winds are the result of an interplay between the South Atlantic High Pressure Cell, a thermal low that forms over southern Africa in summer, coastal lows, and eastward moving extra tropical cyclones (Shannon 1985). In summer, the band of extra tropical cyclones associated with the jetstream moves to the south of its winter position, while the South Atlantic High intensifies and moves approximately 6° to the south (Preston-Whyte and Tyson 1988), creating a pressure gradient over the Benguela region. The presence of the thermal low over the adjacent subcontinent increases the existing pressure gradient, and enhances the equatorward air flow. This seasonal modulation of upwelling favourable winds results in an upwelling season that extends from about September to March (Shannon 1985). During this period, there is also synoptic modulation, provided by wind relaxation or reversal events. These events are either associated with the passage of a cyclone to the south of the continent, or with a coastal low passing along the coast (Shannon 1985).

It will be shown in the following chapter that this coast-wide upwelling is associated with the separation of the water in Saldanha Bay into two distinct layers. In winter the water in the bay is isothermal, but in summer the water separates into two layers. The upper layer is warm and nutrient-depleted, while the lower layer is cold and rich in nutrients. Vertical mixing across the

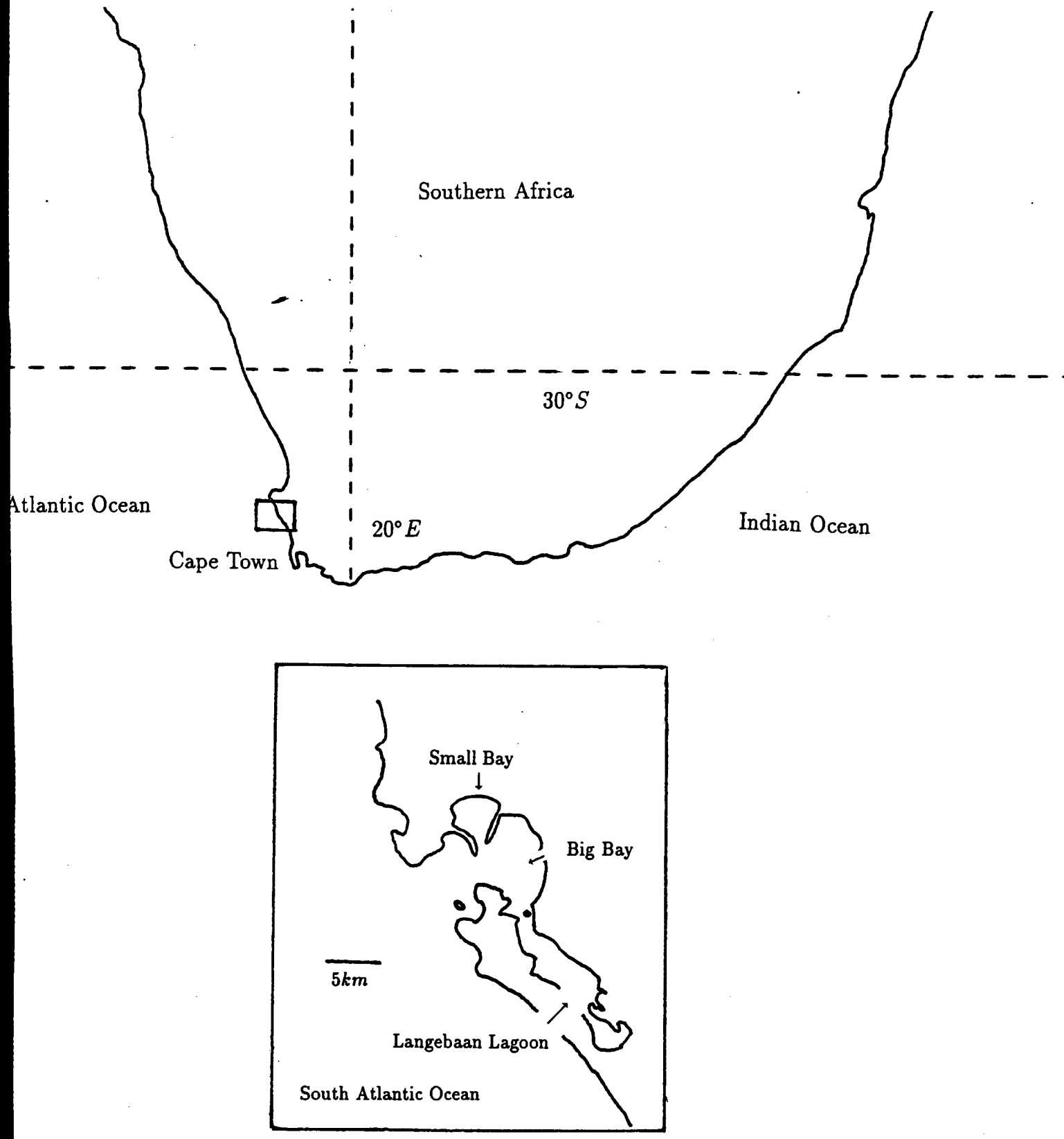

Figure 1.1: A map of southern Africa, with an inset showing the Saldanha Bay system after completion of the harbour works in 1975.

interface separating the two layers will be inhibited by the stability of the strong thermocline. The only exchange that will occur across the thermocline is when water is entrained from one layer into the other. The upper layer is always likely to be the more turbulent of the two layers in this wind-forced system, resulting in one-way entrainment of lower layer water into the upper layer. Any entrainment that does occur in Saldanha Bay should, therefore, result in water properties from the lower layer being injected into the upper layer.

Saldanha Bay has become an extremely important centre for mariculture in South Africa, with important mussel farming and seaweed harvesting industries (Monteiro and Brundrit in press). These industries are highly dependent on maintaining a reasonable water quality within the bay. Maintenance of water quality, however, can only be achieved through carefull management of industries that impact on water quality, to ensure that the carrying capacity of the bay is not exceeded. This, in turn, requires knowledge of the physical processes operating in the bay. Entrainment provides the natural nutrient flux into the upper layer, and so quantification of the amount of entrainment occuring in the bay is essential from a management perspective. In Australia, recent work by D'Adamo et al (1992) has highlighted the effect that stratification, and entrainment, can have on nutrient availability in an embayment.

The main objective of this thesis is, therefore, to attempt to quantify the amount of lower layer water that is entrained into the upper layer of the bay. A secondary objective is to use estimates of entrainment to determine simple budgets of nutrients and heat for the upper layer.

The entrainment concepts of Pollard et al (1973) will be used in order to achieve these objectives. In their work, the velocity shear across the interface, that separates the surface mixed layer from the underlying water, is used to drive entrainment. The crucial argument is that entrainment only begins when the Richardson number has reduced to a critical value, and that entrainment then acts to ensure that the Richardson number never decreases below this critical value. The Pollard et al (1973) model was derived to investigate deepening of the surface mixed layer in the open ocean. In the open ocean, the surface mixed layer will tend to deepen at the beginning of winter, when loss of heat to the atmosphere decreases the stratification to such an extent, that large wind events can result in critical Richardson numbers. The depth of the surface mixed layer offshore is, therefore, likely to be determined by one or two large winter storms. The onset of summer in the Benguela system, with its strong positive surface heat flux, should see the stratification of the upper layer increasing in intensity. This means that subsequent summer wind events are unlikely to lead to mixed layer deepening far offshore. The presence of the coastal boundary, however, may lead to entrainment adjacent to the coast during these upwelling favourable wind events. This idea is investigated by applying the critical Richardson number concept to solutions obtained from a simple model of two layer upwelling. The upwelling model will be restricted to two spatial dimensions. The morphology of Saldanha

Bay (see figure 1.1) can, however, be expected to modify the upwelling response from that of a simple two dimensional model. This is a weakness in the model, which is necessary to keep the problem tractable. The estimates of entrainment that result from the model are used to help determine the nutrient and heat fluxes into the upper layer over synoptic and seasonal time scales.

Chapter 2 is a brief review of the literature pertinent to this study. The chapter begins with a summary of the oceanography of Saldanha Bay, before looking at the model of Pollard et al (1973), and how it might be modified by the presence of a coast and coastal upwelling. Finally, a simple model of two layer upwelling is introduced. Chapter 3 seeks to mate the solutions to the upwelling model with Richardson number concepts about entrainment. Difficulties are encountered, and entrainment can only be approximated near to a coast, with these approximations being used to determine the nutrient and heat budgets for Saldanha Bay. Approximations of the amount of entrainment occuring under different scenarios are presented in chapter 4, and the nutrient and heat budgets are also presented. Chapter 5 is a discussion of what was done in the thesis, and the relevance of this work to Saldanha Bay and similar systems.

Chapter 2

LITERATURE REVIEW

This brief literature review seeks to show that Saldanha Bay is a two layer system during summer, and that the input of nutrients into the biologically important upper layer depends on the entrainment of lower layer water into this upper layer. The concept of shear driven entrainment is introduced in the form of the simple model of Pollard et al (1973), and an indication is given of the effects that a coastal boundary, and the consequent upwelling, may have on the entrainment process. Finally, a simple model of two layer upwelling is examined, so that the shear driven entrainment concepts can be extended to an upwelling region in subsequent chapters.

2.1 Oceanography of Saldanha Bay

In a study prior to the construction of the iron ore jetty in 1975, Shannon and Stander (1977) examined physical and chemical data from Saldanha Bay and Langebaan Lagoon. The authors found that the surface temperature of the bay ranges from $14 - 19°C$, with higher temperatures during summer and lower temperatures in winter. These temperatures are significantly warmer than the typical inshore temperature range of $10 - 14°C$ observed along the west coast in summer, and $12 - 14°C$ in winter (Shannon and Stander 1977). During winter and spring, Shannon and Stander (1977) found a vertically uniform water column, but in summer and autumn, a strong shallow thermocline was observed at some of their stations. These observations are supported by results obtained by Monteiro and Brundrit (1990) from data collected after the iron ore jetty was completed. The authors found that the bay is nearly isothermal in winter, but that a strong thermocline is present between 5 and $10m$ in summer, which tends to turn the bay into a two layer system (see figure 2.1). This layered temperature pattern is not reflected in the salinity of the water. With the exception of Langebaan Lagoon, Shannon and Stander (1977) observed that the salinity in Saldanha Bay showed little spatial or temporal variation, with a mean salinity of about $34.9psu$. The seasonal pattern of stratification has been examined by Monteiro and Brundrit (in press). In spring, the large scale upwelling of water begins along the coast. The inflow of a tongue of this upwelled water, at a temperature of $10 - 12°C$, underneath the warmer bay winter

water creates the initial weak stratification. This initial stratification reduces vertical mixing, and results in enhanced heating of the upper layer by the large surface heat flux, which causes the stratification to increase in intensity. Guastella (1992) found that the daily mean heat flux into the sea at Saint Helena Bay, just to the north of Saldanha Bay, was as high as $315 W.m^{-2}$ in October. Her work suggests that this daily mean heat flux will rise to approximately $340 W.m^{-2}$ in midsummer. Monteiro and Brundrit (in press) discuss the stratification pattern observed during the austral summer of 1994-1995.

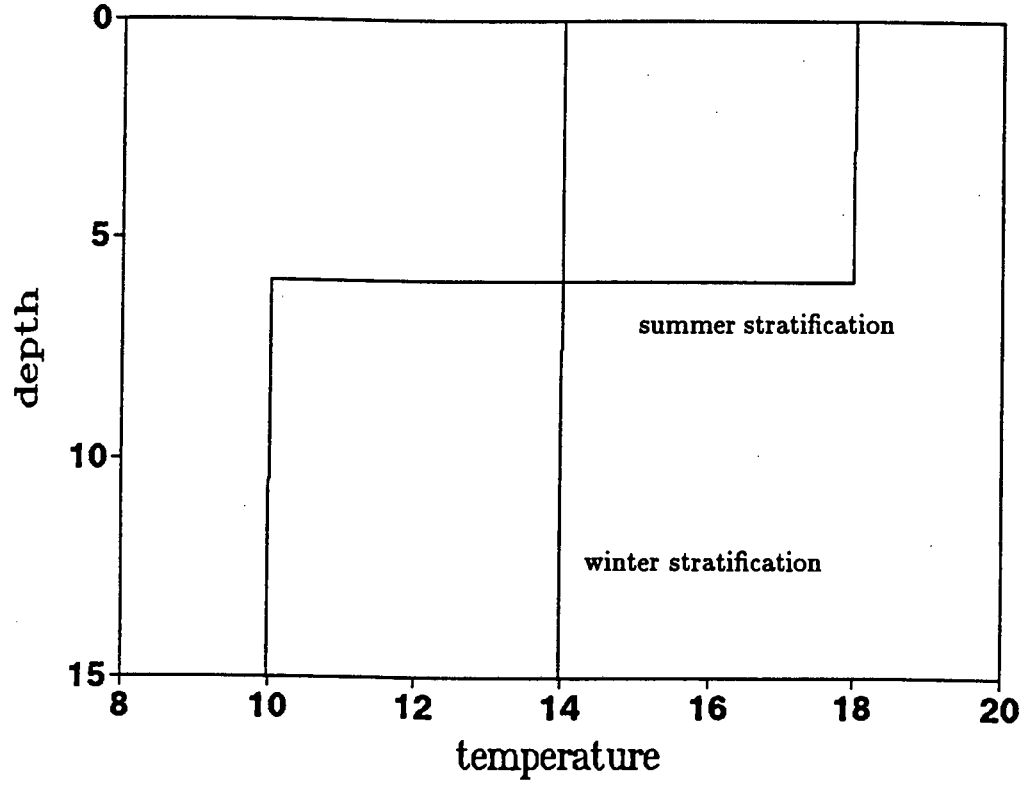

Figure 2.1: A schematic illustrating the difference between the isothermal water column in winter, and the two layer stratification observed in summer.

Upwelling began in August, creating a weakly stratified two layer system in the bay, with a temperature difference of $2 - 3°C$ between the layers. During September the stratification re-

mained reasonably constant, but from October to December the temperature difference increased rapidly to $5 - 6°C$. The temperature difference peaked at $10°C$ from late December to January, and remained at greater than $7°C$ through February. This seasonal stratification pattern has synoptic scale variability superimposed on it (Monteiro and Brundrit, in press), that appears to be driven by the inflow and outflow of the upwelled tongue of water. The variability in the stratification of the bay has a period of 6 to 7 days, which suggests a link with the wind events that drive upwelling in the Benguela system (Monteiro and Brundrit, in press), which exhibit a similar periodicity. During periods when the upwelled tongue of water is absent, the bay is isothermal and has the same temperature as the upper layer when the bay is a two layer system. This is consistent with coastal surface water flowing into the bay to compensate for the withdrawal of the bottom layer. During phases of active upwelling, when the tongue of upwelled water moves into the bay, a compensatory outflow of surface water must occur. It is not certain whether the inflow of the upwelled tongue is a response to the large scale upwelling occuring all along the shelf, or whether it is a compensatory response to a wind driven outflow of surface water from the bay. In either case, the periods of stratification will reduce vertical mixing in the bay.

The currents in the bay are forced by the wind and tide, the relative importance of the two mechanisms changing with depth and position in the bay. Prior to the harbour works, Shannon and Stander (1977) found that tidal currents were particularly strong at the mouth of the bay, and at the junction of the bay and Langebaan Lagoon. A numerical study of the tidal circulation in Saldanha Bay and Langebaan Lagoon was undertaken by the Council for Scientific and Industrial Research (CSIR 1976a, CSIR 1976b). The model was two dimensional, and focused on tidal forcing of the circulation. The relevance of this study can be questioned, however, because the model ignores stratification, and because wind forcing is frequently observed to dominate tidal forcing, in determining the circulation within the bay. Using historical drogue data collected after 1975, Weeks et al (1991a) concluded that wind-forcing dominates tidal-forcing in determining upper layer currents over most of the bay, but that this wind dominance diminishes with depth. In summer, tidal effects are important beneath the thermocline. However, in winter, the wind dominated upper layer extends to the bottom of the bay. Using current meter data collected near the mouth of Small Bay in winter, Weeks et al (1991b) observed an inflow of deep water in response to a shallower outflow of water that was driven by strong winds. This is a similar compensatory flow as occurs in the two layer summer situation. Weeks et al (1991b) highlighted the implications that this wind-driven replacement flow may have for pollution.

The nutrient distribution in the bay indicates that the concentration of nutrients is far higher in the bottom layer than in the upper layer. Monteiro and Brundrit (in press) assert that the surface layer has $[NO_3] \simeq 0\mu M$, while the bottom layer has $[NO_3] > 20\mu M$. Data collected over an eighteen month period, and presented in Shannon and Stander (1977), shows that the mean concentrations of nitrate increase significantly away from the surface. Other nutrients should

display a similar vertical distribution. Whatever nitrate is injected into the upper layer is clearly rapidly utilized by phytoplankton. The only natural source for nitrogen (discounting land based sources for nitrogen) is the bottom layer. In summer, therefore, nitrogen can only be injected into the upper layer during the phases of the synoptic cycle when the bay is a two layer system. This nitrogen injection can be achieved through entrainment of nutrient-rich lower layer water into the upper layer. The turbulent diffusion discussed in Monteiro and Brundrit (in press) is a measure of this entrainment process.

2.2 Entrainment

Entrainment of water, driven by a velocity shear across the interface, into an upper layer will now be considered.

2.2.1 mixed layer deepening

The entrainment of water from below a thermocline into the surface mixed layer was considered by Pollard et al (1973) for a horizontally unbounded ocean. Their model assumed that the mixed layer behaves as a slab with no velocity or temperature gradients. This mixed layer slips freely over a linearly stratified lower layer. A wind stress is switched on, which drives upper layer currents, and the resultant current shear at the base of the mixed layer leads to a deepening of the mixed layer through entrainment. According to Pollard et al (1973) this entrainment is achieved through breaking interfacial waves, when the velocity shear across the interface has made the waves sufficiently unstable. The crucial element of the model is a closure scheme involving the Richardson number, which is a ratio of turbulence supressing buoyancy effects to turbulence enhancing shear effects. The Richardson number that Pollard et al (1973) use is:

$$Ri = \frac{gH_1\frac{\Delta\rho}{\rho}}{(\Delta u)^2} \tag{2.1}$$

where g is gravitational acceleration
where $\Delta\rho$ is the density of the water
where $\Delta\rho$ is the density difference across the thermocline
where H_1 is the depth of the surface mixed layer
and Δu is the velocity shear across the thermocline

When this Richardson number reaches a critical value, entrainment increases the depth of the mixed layer so as to ensure that the Richardson number never becomes sub-critical. Pollard et al (1973) give three different explanations for their choice of 1 as the critical Richardson number. Their most persuasive argument relates the change in kinetic and potential energy of the upper layer to the rate of working by the wind on the mean flow. However, observations by Krauss (1981) of thermocline erosion in the Baltic, and laboratory experiments quoted in Pollard et al

(1973), suggest that the critical Richardson number is 0.25. Pollard et al (1973) solve the open ocean momentum equations for an ocean that is initially at rest and substitute their solutions into the shear terms of the Richardson number by assuming that the water beneath the surface mixed layer has no momentum. The authors then determine $\Delta\rho$ by assuming that density changes are due to temperature alone, and that the surface heat flux is negligble. Using a value of 1 as the critical Richardson number, the depth of the surface mixed layer is given by:

$$H_1 = (\frac{X_s}{\rho})^{\frac{1}{2}}[\frac{4(1-\cos ft)}{f^2N^2}]^{\frac{1}{4}} \qquad (2.2)$$

where f is the coriolis parameter
where N is the Brunt-Väisala frequency
and where X_s is the X component of the wind stress

Examination of equation 2.2 indicates that the surface mixed layer will deepen until $t = \frac{\pi}{f}$, when the deepening is stopped by rotation. For $t > \frac{\pi}{f}$, H_1 will be constant, because the water cannot unmix. Supporting evidence for this simple model comes from the observations of mixed layer deepening made by Halpern (1974) in the Northeast Pacific Ocean. Extending the model to include arbitrary initial stratification and currents is possible.

An important component of the velocity shear that deepens the mixed layer is due to inertial oscillations. When a steady wind blows over a resting ocean, the water movement is initially in the same direction as the wind. The coriolis effect, however, ultimately causes the movement to be given by the sum of a steady Ekman transport to the left of the wind (in the southern hemisphere), and a rotating inertial circle of the same amplitude (Gill 1982). These inertial oscillations are often observed in the ocean, and tend to have horizontal coherence scales of the order of tens of kilometres, and vertical coherence scales of tens of meters (Anderson et al 1983). The model of Pollard (1970) suggests that inertial oscillations decrease rapidly with depth beneath the surface mixed layer. This is supported by observations in the open ocean that indicate that near-inertial energy decreases with depth (Anderson et al 1983). Because the oscillations are largely confined to the surface mixed layer, they result in a significant increase in the shear across the interface.

If the wind is not steady, or if the ocean is not initially at rest, the amplitude of the inertial oscillation can change dramatically. Either constructive or destructive interference between the wind and the inertial oscillation can occur (Pollard and Millard 1970). In one extreme case, a shift in the wind can completely eliminate existing inertial oscillations. On the other hand, if the wind stress is changing at a similar frequency to the inertial frequency, a resonant oscillation can occur. The possibility of resonant inertial oscillations is significant in Saldanha Bay, because the bay lies at a latitude where the inertial period is similar to the diurnal period of land-sea breezes. The land-sea breeze component of the wind stress may result in resonant oscillations (Boyd 1981). A resonant oscillation will result in a velocity shear that increases with time, possibly leading to

very deep surface mixed layers. The effect of land-sea breezes will normally, however, be confined to a region near the coast, and the coastal boundary may impact on the inertial oscillations.

2.2.2 coastal effects

Pollard et al (1973) limit their study to one spatial dimension, or rather to the open ocean, thereby excluding any boundary effects. It might be expected, however, that the presence of a horizontal boundary will have a significant effect on the process of entrainment. Because no flow is possible across it, currents perpendicular to the boundary will result in vertical movements of the water surface, and regions of convergence or divergence. These convergent and divergent regions have to be compensated for by vertical movements of the interface separating the layers, and flow in the lower layer. This lower layer replacement flow will be in the opposite direction to the flow in the upper layer, enhancing the velocity shear across the interface. In addition, the vertical movements of the water surface and interface will drive geostrophic longshore currents parallel to the coast. The changes that a coastal boundary makes to the shear terms, as well as the vertical movements of the water surface and interface, will alter the Richardson number from the open ocean case.

The establishment of geostrophic currents by the coastal boundary will be accompanied by a second system of inertial oscillations, this time in the lower layer, which will be 180° out of phase with the oscillations in the upper layer (Krauss 1981). From observations made in the middle of the Baltic Sea, Krauss (1981) concluded that the contribution of the mean current to shear across the base of the mixed layer was negligible compared to the shear caused by the out of phase inertial oscillations. Nearer the coast, however, the oscillations may be negatively affected by the presence of the coastal boundary. Observations from the Oregon shelf (Anderson et al 1983) indicate that there is much less near-inertial energy over the continental shelf than at similar depths offshore, and that the motion is less persistent over the shelf. Supporting this is the two layer modelling work of Millot and Crepon (1981), which will be investigated in the following section, that shows that the amplitude of wind driven inertial oscillations in both layers decreases to zero at the coast. Their work also indicates that inertial oscillations will decay with time on the order of $(ft)^{-\frac{1}{2}}$ in the presence of a coastal boundary. These effects suggest that inertial oscillations may play a smaller role in enhancing shear across an interface near a boundary, than they do far offshore.

Largier (1990) investigated the effect of interfacial shear, generated by internal tides and wind driven motion, on the depth of the surface mixed layer. In considering the effect of wind driven motion, the author adapted the wind driven deepening model of Pollard et al (1973) to account for a finite water depth and the presence of a coastal boundary. This was done by introducing a

factor of $\frac{h_1 h_2}{h_1+h_2}$ (where h_1 and h_2 are the depths of the upper and lower layers respectively) into the Richardson number as the suitable depth scale for the velocity shear, and by parameterizing the flow in the lower layer by a ratio, estimated from field data, of upper layer wind driven flow to lower layer wind driven flow. These adaptations to the Pollard et al (1973) model do not, however, take into account the rise or fall of the interface between the two layers, which causes the lower layer flow. Observations of the middle and outer shelf in coastal upwelling regions by Lentz (1992), showed that the depth of the surface mixed layer was consistent with the model of Pollard et al (1973), when there is no surface heat flux. This led the author to postulate that the effects of the large surface heat flux, that characterises upwelling regions, may be balanced by the offshore advection of heat associated with upwelling. Upwelling may, therefore, simplify the physics of mixed layer deepening by eliminating the dependence on the surface heat flux. Lentz (1992) found that the maximum offshore shear was measured at the base of the mixed layer, which is what would be expected. The maximum longshore shear, however, was found near the water surface, and was consistent with a constant stress log-layer response of the ocean to the wind stress. The fact that there was no significant longshore shear at the base of the mixed layer, is an indication that the measurements were made sufficiently far from the coast that upwelling of the interface was insignificant. This is supported by the fact that measurements of the offshore mass transport were in good agreement with open ocean Ekman theory. The condition that the offshore flow must reduce to zero at the coast clearly did not impact on the measurements made by Lentz (1992).

These observations suggest that the model of Pollard et al (1973) is suitable for use on the middle to outer shelf in coastal upwelling regions. In Saldanha Bay, however, the interest is on processes occuring immediately adjacent to the coastal boundary. In order for shifts in the interface to be taken into consideration in the dynamics of mixed layer deepening, and in order to remove the reliance on field measurements of shear, a simple upwelling model will now be introduced.

2.3 A simple model of two layer upwelling

A simple model of two layer upwelling is required to provide the surface mixed layer depth and velocity shear terms necessary for the calculation of the Richardson number.

2.3.1 derivation of the equations

The derivation of the equations governing a two layer system near a horizontal boundary will follow Gill (1982). Initially the system will be at rest, with an upper layer of depth h_1 overlying a lower layer of thickness h_2. The total water depth (H) will be:

$$H = h_1 + h_2 \tag{2.3}$$

Variables in the upper layer will be represented by the subscript 1, while those in the lower layer will have the subscript 2. The displacements of the surface and the interface will, therefore, be given by ϵ_1 and ϵ_2 respectively. Using a Cartesian coordinate system (where x and y are in the horizontal and z in the vertical plane), the momentum equations have the form:

$$\frac{\partial u}{\partial t} - fv = -\frac{1}{\rho}\frac{\partial p}{\partial x} + \frac{1}{\rho}\frac{\partial X_s}{\partial z} \tag{2.4}$$

$$\frac{\partial v}{\partial t} + fu = -\frac{1}{\rho}\frac{\partial p}{\partial y} + \frac{1}{\rho}\frac{\partial Y_s}{\partial z} \tag{2.5}$$

and the hydrostatic equation has the form:

$$\frac{\partial p}{\partial z} = -\rho g \tag{2.6}$$

where u and v are the components of the current velocity in the x and y directions respectively where X_s and Y_s are the components of the wind stress in the x and y directions respectively and where p is pressure

From the hydrostatic equation:

$$p_1 = \rho_1 g(\epsilon_1 - z) \tag{2.7}$$

$$p_2 = \rho_1 g(h_1 - \epsilon_2 + \epsilon_1) + \rho_2 g(\epsilon_2 - h_1 - z) \tag{2.8}$$

therefore, if the X component momentum equations are considered:

$$\frac{\partial p_1}{\partial x} = \rho_1 g \frac{\partial \epsilon_1}{\partial x} \tag{2.9}$$

$$\frac{\partial p_2}{\partial x} = \rho_1 g \frac{\partial \epsilon_1}{\partial x} + g(\rho_2 - \rho_1)\frac{\partial \epsilon_2}{\partial x} \tag{2.10}$$

which means that:

$$\frac{\partial u_1}{\partial t} - fv_1 = -g\frac{\partial \epsilon_1}{\partial x} + \frac{1}{\rho_1}\frac{\partial X_s}{\partial z} \tag{2.11}$$

$$\frac{\partial u_2}{\partial t} - fv_2 = -\frac{g\rho_1}{\rho_2}\frac{\partial \epsilon_1}{\partial x} - \frac{g(\rho_2 - \rho_1)}{\rho_2}\frac{\partial \epsilon_2}{\partial x} + \frac{1}{\rho_2}\frac{\partial X_s}{\partial z} \tag{2.12}$$

the reduced gravity ($\hat{g}$) can be defined as:

$$\hat{g} = \frac{g(\rho_2 - \rho_1)}{\rho_2} \tag{2.13}$$

If the assumption is now made that the stress due to the wind is confined to the upper layer, and that this upper layer moves as a slab:

$$\frac{\partial X_s}{\partial z} = \frac{X_s}{h_1} \tag{2.14}$$

if the Boussinesq approximation is made:

$$\frac{\rho_1}{\rho_2} \simeq 1 \tag{2.15}$$

then the momentum equations become:

$$\frac{\partial u_1}{\partial t} - fv_1 = -g\frac{\partial \epsilon_1}{\partial x} + \frac{X_s}{\rho_1 h_1} \tag{2.16}$$

$$\frac{\partial u_2}{\partial t} - fv_2 = -g\frac{\partial \epsilon_1}{\partial x} - \hat{g}\frac{\partial \epsilon_2}{\partial x} \tag{2.17}$$

The bottom layer equation can now be subtracted from the upper layer equation, and the X and Y component shears can be defined as:

$$\hat{u} = u_1 - u_2 \tag{2.18}$$

$$\hat{v} = v_1 - v_2 \tag{2.19}$$

The X component momentum equation can thus be written as:

$$\frac{\partial \hat{u}}{\partial t} - f\hat{v} = \hat{g}\frac{\partial \epsilon_2}{\partial x} + \frac{X_s}{\rho_1 h_1} \tag{2.20}$$

similarly, the Y component equation is given by:

$$\frac{\partial \hat{v}}{\partial t} + f\hat{u} = \hat{g}\frac{\partial \epsilon_2}{\partial y} + \frac{Y_s}{\rho_1 h_1} \tag{2.21}$$

The continuity equation can be derived through observing that for a box with a fixed base, the change in mass with time will equal the difference between the mass inflow and the mass outflow. If the "thickness" of the box is given by γ, then the continuity equation will be given by:

$$\frac{\partial \gamma}{\partial t} = -\frac{\partial}{\partial x}(u\gamma) - \frac{\partial}{\partial y}(v\gamma) \tag{2.22}$$

The "thickness" of the two layers will be:

$$\gamma_1 = h_1 + \epsilon_1 - \epsilon_2 \tag{2.23}$$

$$\gamma_2 = h_2 + \epsilon_2 \tag{2.24}$$

The two continuity equations are, therefore:

$$\frac{\partial}{\partial t}(h_1 + \epsilon_1 - \epsilon_2) + \frac{\partial}{\partial x}(u_1 h_1 + u_1\epsilon_1 - u_1\epsilon_2) + \frac{\partial}{\partial y}(v_1 h_1 + v_1\epsilon_1 - v_1\epsilon_2) = 0 \tag{2.25}$$

$$\frac{\partial}{\partial t}(h_2 + \epsilon_2) + \frac{\partial}{\partial x}(u_2 h_2 + u_2\epsilon_2) + \frac{\partial}{\partial y}(v_2 h_2 + v_2\epsilon_2) = 0 \tag{2.26}$$

These equations can be simplified through neglecting the products of small quantities. If $\frac{\partial}{\partial x}$ and $\frac{\partial}{\partial y}$ of $u\epsilon_1, v\epsilon_1, u\epsilon_2$, and $v\epsilon_2$ are all small, and if the rigid lid approximation:
$\frac{\partial \epsilon_1}{\partial t} << \frac{\partial \epsilon_2}{\partial t}$
is made, the equations become:

$$-\frac{\partial \epsilon_2}{\partial t} + h_1(\frac{\partial u_1}{\partial x} + \frac{\partial v_1}{\partial y}) = 0 \quad (2.27)$$

$$\frac{\partial \epsilon_2}{\partial t} + h_2(\frac{\partial u_2}{\partial x} + \frac{\partial v_2}{\partial y}) = 0 \quad (2.28)$$

These can be combined into one equation, by dividing the upper and lower equations by h_1 and h_2 respectively, and subtracting the lower layer equation from that of the upper layer. The full set of equations governing the two layer fluid are:

$$\frac{\partial \epsilon_2}{\partial t} - \frac{h_1 h_2}{h_1 + h_2}(\frac{\partial \hat{u}}{\partial x} + \frac{\partial \hat{v}}{\partial y}) = 0 \quad (2.29)$$

$$\frac{\partial \hat{u}}{\partial t} - f\hat{v} = \hat{g}\frac{\partial \epsilon_2}{\partial x} + \frac{X_s}{\rho_1 h_1} \quad (2.30)$$

$$\frac{\partial \hat{v}}{\partial t} + f\hat{u} = \hat{g}\frac{\partial \epsilon_2}{\partial y} + \frac{Y_s}{\rho_1 h_1} \quad (2.31)$$

If a wind stress X_s is applied parallel to a horizontal boundary at $y = 0$, and if $Y_s = 0$, the equations become:

$$\frac{\partial \epsilon_2}{\partial t} - \frac{h_1 h_2}{h_1 + h_2}\frac{\partial \hat{v}}{\partial y} = 0 \quad (2.32)$$

$$\frac{\partial \hat{u}}{\partial t} - f\hat{v} = \frac{X_s}{\rho_1 h_1} \quad (2.33)$$

$$\frac{\partial \hat{v}}{\partial t} + f\hat{u} = \hat{g}\frac{\partial \epsilon_2}{\partial y} \quad (2.34)$$

These can be combined into one equation by taking $\frac{\partial}{\partial y}$ of the continuity equation, and $\frac{\partial}{\partial t}$ of the Y component momentum equation. After substitution, the resultant wave equation for the offshore shear is:

$$\frac{\partial^2 \hat{v}}{\partial t^2} - c_2^2\frac{\partial^2 \hat{v}}{\partial y^2} + f^2\hat{v} = \frac{fX_s}{\rho_1 h_1} \quad (2.35)$$

According to Gill (1982), this equation also governs the one layer storm surge problem, if $\hat{v}$ is replaced by v_1 (the offshore velocity in the layer), and c_2 (the baroclinic wave velocity) is replaced by c_1 (the barotropic wave velocity). The wave velocities are given by:

$$c_1 = [gH]^{\frac{1}{2}} \quad (2.36)$$

$$c_2 = [\hat{g}\frac{h_1 h_2}{H}]^{\frac{1}{2}} \quad (2.37)$$

While the barotropic and baroclinic Rossby Radii are given by:

$$r_1 = \frac{c_1}{f} \tag{2.38}$$

$$r_2 = \frac{c_2}{f} \tag{2.39}$$

2.3.2 a solution for steady offshore shear

A solution can easily be obtained if it is assumed that the offshore shear ($\hat{v}$) is steady (Gill 1982). Equation 2.35 then becomes:

$$\frac{\partial^2 \hat{v}}{\partial y^2} - \frac{f^2}{c_2^2}\hat{v} = \frac{fX_s}{\rho_1 h_1 c_2^2} \tag{2.40}$$

which is a non-homogenous second order partial differential equation.
This equation can be solved by the method of variation of parameters (if f is assumed to be constant), to obtain a general solution:

$$\hat{v} = k_1 \exp^{\frac{fy}{c_2}} + k_2 \exp^{\frac{-fy}{c_2}} - \frac{X_s}{f\rho_1 h_1} \tag{2.41}$$

where k_1 and k_2 are constants

The boundary conditions that can be applied are:

- That the offshore shear is bounded away from the coast.
  because $\exp^{\frac{fy}{c_2}} \rightarrow \infty$ as $y \rightarrow \infty$
  $k_1 \simeq 0$ for $\hat{v}$ to remain bounded

- That there is no flow through the boundary.
  $\hat{v} = 0$ at $y = 0$

These boundary conditions give a final solution for $\hat{v}$, with $\hat{u}$ and ϵ_2 obtained through substituting back into the original equations:

$$\hat{v} = -\frac{X_s}{\rho_1 h_1 f}(1 - \exp^{-\frac{y}{r_2}}) \tag{2.42}$$

$$\hat{u} = \frac{X_s}{\rho_1 h_1} \exp^{-\frac{y}{r_2}} t \tag{2.43}$$

$$\epsilon_2 = -\frac{c_2 X_s}{\rho_1 h_1 \hat{g}} \exp^{-\frac{y}{r_2}} t \tag{2.44}$$

By definition, the offshore shear in this solution is steady. The offshore shear does, however, increase exponentially from zero at the coast to the value of the steady Ekman transport infinitely far from the shore. The upper layer divergence implied by this result, causes shifts in the interface separating the two layers, and a longshore shear that responds to the sloping interface. This interface displacement, and the associated longshore shear, increase linearly with time, which

will cause the Richardson number to decrease with time. An important point to note is that the steady equations have no transients, the influence of inertial oscillations has been removed by assuming that the offshore shear is steady. Because these oscillations play an important role in the reduction of the Richardson number in the open ocean case studied by Pollard et al (1973), it would be usefull to obtain a solution in which the transients are retained.

2.3.3 a transient solution

The full, time dependent, equation (equation 2.35) can be solved by the method of taking Laplace transforms. The inversion of the transform, however, leads to inconvenient algebra. Anderson and Gill (1979) give Crepons solution to the one layer problem. In the absence of a coastline, the solution is independent of the offshore distance y:

$$v_1 = \frac{X_s}{\rho_1 h_1 f}(\cos ft - 1) \tag{2.45}$$

(in the two layer situation v_1 would be replaced by $\hat{v}$)
Anderson and Gill (1979) observe that a coastline will modify this solution with boundary effects that propogate away from the coast at speed c_1. The full solution is given by:

$$\begin{aligned} v_1 = & -\frac{X_s}{\rho_1 h_1 f}(1 - \cos ft) \\ & + \frac{X_s}{\rho_1 h_1 f}\{\exp^{-\frac{fy}{c_1}} - \cos ft + \frac{2f^2}{\pi}\int_f^\infty \frac{\cos(st)\sin[(s^2-f^2)^{\frac{1}{2}}\frac{y}{c_1}]}{s(s^2-f^2)}\,ds\}H(t - \frac{y}{c_1}) \end{aligned} \tag{2.46}$$

The first term is the solution in the absence of a boundary, the second term, therefore, represents the boundary effect. The Heaviside function $H(t - \frac{y}{c_1})$ shows that the boundary effect is zero for $t < \frac{y}{c_1}$. What this means for the two layer case is that $\hat{v}$ (the offshore velocity shear) at a point is given by the "open ocean" solution, until the baroclinic wave front passes, whereafter it is modified by boundary effects. The longshore shear will also be given by the "open ocean" solution, and the interface displacement will be zero, until the baroclinic wave passes.

The actual two layer problem has been considered by Millot and Crepon (1981). From their results, Baines (1986) determines that the motion initially displays "open ocean" behaviour, which is modified by a baroclinic and a barotropic wave propogating from the coast. Baines (1986) identifies three regimes (where r_1 and r_2 are respectively the barotropic and baroclinic Rossby Radii):

- $ft < \frac{y}{r_1}$
  Here the flow consists of the "open ocean" solution. There is Ekman transport with superimposed inertial oscillations in the upper layer. There is no pressure gradient, no displacement of the interface, and no motion in the lower layer.

- $\frac{y}{r_1} < ft < \frac{y}{r_2}$
  The barotropic wave front has passed, causing motion and inertial oscillations in the lower layer. There are, however, no oscillations in the interface depth.

- $\frac{y}{r_2} < ft$
  The baroclinic wave front has passed, causing oscillations in the interface depth.

The results contained in Anderson and Gill (1979), which show that the shear and interface depth are only altered from the "open ocean" solution by the passage of the baroclinic wave, allow the merging of the first two regimes. Although the passage of the barotropic wave has an effect on the absolute velocities in both layers, it does not affect the shear and interface depth, which is what determines the Richardson number. In considering entrainment, therefore, the two important regimes are before the baroclinic wave passes, when the shear is given by the "open ocean" solution and the interface displacement is zero, and after the baroclinic wave has passed.

Once the baroclinic wave has passed, the shear, as well as the interface and surface displacements are given by Millot and Crepon (1981). The authors use a linearized two layer model with negligible interfacial and bottom stress, and no rigid lid approximation. Otherwise the equations are as in Gill (1982), with a constant wind blowing parallel to a shore at $y = 0$. Millot and Crepon (1981) solve the equations using Laplace transforms, and make use of an asymptotic expansion in the simplification of their results that is only valid for $ft > \frac{y}{r_2}$. In other words, their solution is only valid for points inside the baroclinic wave front. Millot and Crepon (1981) provide solutions for the offshore and longshore velocities in both layers, as well as the surface and interface displacements. The surface displacement will be ignored, however, because it is very much less than the interface displacement, and consequently plays a small role in determining the Richardson number. Because the area of interest is relatively close to the coast, the additional assumption that $y < r_2 << r_1$ can be made. The simplified equations that result are:

$$v_1 = -\frac{X_s}{\rho_1 h_1 f}\left(\frac{h_2}{H}\right)\left\{1 - \exp^{-\frac{y}{r_2}} + \left(\frac{y}{r_2}\right)(ft)^{\frac{-1}{2}}\left(\frac{2}{\pi}\right)^{\frac{1}{2}}\left[\sin\left(ft - \frac{\pi}{4}\right)\right]\right\} \quad (2.47)$$

$$u_1 = \frac{X_s}{\rho_1 h_1 f}\left(\frac{h_2}{H}\right)\left\{\frac{h_1}{h_2} ft + \exp^{-\frac{y}{r_2}} ft + \left(\frac{y}{r_2}\right)(ft)^{\frac{-1}{2}}\left(\frac{2}{\pi}\right)^{\frac{1}{2}}\left[\cos\left(ft - \frac{\pi}{4}\right)\right]\right\} \quad (2.48)$$

$$v_2 = \frac{X_s}{\rho_1 H f}\left\{1 - \exp^{-\frac{y}{r_2}} + \left(\frac{y}{r_2}\right)(ft)^{\frac{-1}{2}}\left(\frac{2}{\pi}\right)^{\frac{1}{2}}\left[\sin\left(ft - \frac{\pi}{4}\right)\right]\right\} \quad (2.49)$$

$$u_2 = \frac{X_s}{\rho_1 H f}\left\{ft - \exp^{-\frac{y}{r_2}} ft - \left(\frac{y}{r_2}\right)(ft)^{\frac{-1}{2}}\left(\frac{2}{\pi}\right)^{\frac{1}{2}}\left[\cos\left(ft - \frac{\pi}{4}\right)\right]\right\} \quad (2.50)$$

$$\epsilon_2 = \left(\frac{X_s}{\rho_1 c_1 f}\right)\left(\frac{h_2}{H}\right)\left\{ft\left(1 - \frac{c_1}{c_2}\exp^{-\frac{y}{r_2}}\right) + \left(\frac{c_1}{c_2} - 1\right)(ft)^{\frac{-1}{2}}\left(\frac{2}{\pi}\right)^{\frac{1}{2}}\cos\left(ft - \frac{\pi}{4}\right)\right\} \quad (2.51)$$

From these equations it is easy to calculate the velocity shear. If the equations for velocity shear and interface displacement are rearranged, their relationship to the steady offshore shear solutions found in Gill (1982) can be shown. The shear equations are:

$$\hat{v} = -\left(\frac{X_s}{\rho_1 h_1 f}\right)\left(1 - \exp^{-\frac{y}{r_2}}\right) - \left(\frac{X_s}{\rho_1 h_1 f}\right)\left(\frac{y}{r_2}\right)(ft)^{\frac{-1}{2}}\left(\frac{2}{\pi}\right)^{\frac{1}{2}}\sin\left(ft - \frac{\pi}{4}\right) \quad (2.52)$$

$$\hat{u} = (\frac{X_s}{\rho_1 h_1 f})(\exp^{-\frac{y}{r_2}})ft + (\frac{X_s}{\rho_1 h_1 f})(\frac{y}{r_2})(ft)^{\frac{-1}{2}}(\frac{2}{\pi})^{\frac{1}{2}}\cos(ft - \frac{\pi}{4}) \quad (2.53)$$

If the ratio of $\frac{c_2}{c_1}$ is small, the equation for the interface displacement can be written as:

$$\epsilon_2 = -(\frac{c_2 X_s}{\rho_1 h_1 \hat{g}})\exp^{-\frac{y}{r_2}} t + (\frac{X_s}{\rho_1 h_1 f})(\frac{c_2}{\hat{g}})(ft)^{\frac{-1}{2}}(\frac{2}{\pi})^{\frac{1}{2}}\cos(ft - \frac{\pi}{4}) \quad (2.54)$$

From these velocity shear equations, it can be seen that the first term corresponds to the steady offshore shear solution given in equations 2.42 and 2.43, while the second term represents the inertial oscillation. The amplitude of the oscillation is given by the term $(\frac{X_s}{\rho_1 h_1 f})(\frac{y}{r_2})(ft)^{\frac{-1}{2}}(\frac{2}{\pi})^{\frac{1}{2}}$. Both the longshore and offshore shear oscillations are of the same magnitude. The amplitude of the oscillations increases linearly away from the coast (although it must be remembered that the solution is only valid inside the baroclinic wave front). It is also clear that the oscillations decay with time, on the order of $(ft)^{\frac{-1}{2}}$. In the equation for the interface displacement (equation 2.54), the first term is again the steady offshore shear solution (equation 2.44), while the second term is oscillatory. These oscillations also decay with time according to $(ft)^{\frac{-1}{2}}$. Unlike the case for the shear terms, however, the amplitude of the oscillations is independent of the offshore scale.

2.4 Summary

This literature review has demonstrated that Saldanha Bay takes on the characteristics of a two layer system during summer. A warm nutrient-depleted upper layer overlies a cold nutrient-rich lower layer. The shear produced by the wind driven processes that cause the inflow of the cold lower layer, can be expected to lead to entrainment of lower layer water by the upper layer. These concepts of shear driven entrainment, and the possible effects of a coastal boundary on the entrainment have been investigated. In order to further investigate these effects, a simple model of two layer coastal upwelling, which is appropriate for Saldanha Bay, has been introduced. Solutions to the model give the shear terms and interface displacements near a boundary. These results will now be used to investigate shear driven entrainment near a coastline. The chief contribution of this thesis to the literature will be the mating of entrainment concepts to an upwelling model.

Chapter 3

METHODOLOGY

This chapter seeks to mate the shear driven entrainment concepts of Pollard et al (1973) to a simple model of two layer upwelling, in order to attempt to quantify the entrainment that takes place while upwelling is occuring.

Far offshore, the entrainment of water into an upper layer is covered by the work of Pollard et al (1973). The Richardson number considered in the previous chapter, however, was for a lower layer that is linearly stratified. In order to extend the model to the two layer situation that was presented in the upwelling model of the previous chapter, the Richardson number (equation 2.1) can be rewritten as:

$$Ri = \frac{\hat{g} H_1}{\hat{u}^2 + \hat{v}^2} \tag{3.1}$$

In this form, the numerator of the Richardson number represents the stratification terms, while the denominator represents the velocity shear terms. Because there will be no upwelling of the interface far offshore, $H_1 = h_1$ before the Richardson number becomes critical. The open ocean shear equations will simply be given by:

$$\hat{u} = \frac{X_s}{\rho_1 h_1 f} \sin ft \tag{3.2}$$

$$\hat{v} = \frac{X_s}{\rho_1 h_1 f} (\cos ft - 1) \tag{3.3}$$

As Pollard et al (1973) noted, these shear terms reach a maximum at $t = \frac{\pi}{f}$. In order for entrainment to occur, the maximum shear must be greater than the initial stratification terms, otherwise the Richardson number will never become critical. A ratio F can be defined by comparing the maximum shear and the stratification terms from the Richardson number. This ratio depends on initial conditions and will later prove valuable. In order for the Richardson number to eventually become critical far offshore:

$$F = \frac{(\frac{X_s}{\rho_1})^2}{(\hat{g} h_1)(h_1 f)^2} \geq \frac{1}{4} \tag{3.4}$$

The crucial variable F is a ratio between the effects of the wind stress and the stratification. As can readily be seen, F depends very sensitively on the initial upper layer depth. This result implies that under light wind conditions and strong stratification (small F), the Richardson number will not become critical and entrainment will never occur far offshore. High winds and weak stratification (large F) will, however, result in a critical Richardson number and entrainment. Pollard et al (1973) propose that their model covers, at most, a few days in the life of the seasonal thermocline. This suggests that an annual large wind event establishes the depth of the upper layer far offshore. In the upwelling model, this depth is represented by the initial upper layer depth (h_1). The role of the large surface heat flux in increasing the stratification between the layers as summer progresses, means that subsequent wind events tend not to result in entrainment far offshore (that is $F < \frac{1}{4}$). The presence of the coastal boundary may, however, alter the Richardson number and cause entrainment near to the coast during subsequent upwelling-favourable wind events. If entrainment does not occur far offshore during these events, the upwelling model of the previous chapter can be used to examine coastal entrainment. The model will not, however, be valid if $F > \frac{1}{4}$. The model is not valid when the model of Pollard et al (1973) predicts deepening of the surface mixed layer. In this model entrainment only occurs because of the divergence in the upper layer.

The bulk of the remainder of this chapter is concerned with investigating entrainment near to the coast, that is within a baroclinic radius of the coast. The first section of the chapter shows that the inertial oscillations which are so important in the open ocean model of Pollard et al (1973), have little effect on entrainment near to the coast, so long as the initial depth of the upper layer is reasonably large (of the order of $10m$). This allows the solutions to the steady offshore shear model to be used to investigate entrainment near to the coast. These equations are scaled, and the time that it takes the Richardson number to become critical is determined. Once the Richardson number has become critical, entrainment must proceed to ensure that the Richardson number never becomes subcritical. It will be shown that entrainment affects the Richardson number not only by deepening the upper layer, but also by reducing the longshore shear. Entrainment and upwelling of the interface interact to maintain the critical Richardson number. An equation is derived to determine the level of entrainment that must take place to keep the Richardson number critical. Unfortunately, solving this equation would prove very difficult, and so maximum and minimum constraints on the amount of entrainment are determined numerically.

3.1 The effect of inertial oscillations on the Richardson number

The solution obtained by Millot and Crepon (1981) to the two layer upwelling problem, which was discussed in the previous chapter, clearly shows that the oscillations that occur in velocity shear and the interface depth, decay with time. As time progresses, therefore, the solution for steady offshore shear will become an increasingly good approximation to the full solution of Mil-

lot and Crepon (1981). If the difference between the steady offshore shear and the full solutions has become small by the time that the Richardson number has reduced to its critical value, then the steady offshore shear solution can be used as a proxy for the full solution when studying entrainment.

The Richardson number for a two layer system was given by equation 3.1. When upwelling favourable winds are blowing, and $F < \frac{1}{4}$, the shear terms and the surface mixed layer depth can be obtained from the solutions of Millot and Crepon (1981) and Gill (1982), for the situation before the Richardson number becomes critical. The surface mixed layer depth will be given by:

$$H_1 = h_1 - \epsilon_2 \tag{3.5}$$

Initially, the Richardson number is infinitely high, because the shear terms are zero at time $t = 0$. Once the wind stress is switched on, however, the Richardson number will immediately begin decreasing towards its critical value, as the velocity shear across the interface becomes established, and the interface begins to shoal.

It was shown in the previous chapter that there are effectively two regimes under which the Richardson number can reduce to its critical value. Regime one will occur at points where the critical value is reached before the baroclinic wave has passed, while regime two will occur at points inside the propogating baroclinic wave. Points outside the propogating baroclinic wave have shear and interface displacements that are unaffected by the coast. In order for the Richardson number to become critical, $F \geq \frac{1}{4}$. This means that the situation is identical to that investigated by Pollard et al (1973), and will not be considered any further.

In most situations near to the coast, the Richardson number will reduce to its critical value in regime two, where the shear terms and interface displacement are given by the solution of Millot and Crepon (1981). The oscillatory shear and upper layer depth terms will have the effect of causing oscillations in the Richardson number, as it reduces to its critical value. Oscillations in the upper layer depth will contribute to the oscillations in the Richardson number, but these oscillations will be around some steady Richardson number. The oscillatory shear terms, however, will cause the mean total shear to be greater than in the steady case, leading to a Richardson number that reduces more rapidly than in the steady case. It was shown in the previous chapter that the oscillations in the offshore and longshore shear decrease to zero as the coast is approached. Near the coast, therefore, the difference in the Richardson number for the steady offshore shear solution and the full time dependent solution is chiefly due to the oscillations in upper layer depth. Because the oscillation in the upper layer depth is positive for $ft < \frac{3\pi}{4}$, the Richardson number at the coast initially reduces more rapidly in the steady solution than in the time dependent one. The opposite is true for $\frac{3\pi}{4} < ft < \frac{7\pi}{4}$. Away from the coast, the effects of the oscillations in longshore and offshore shear will be felt in the Richardson number. The effect of these oscillations

is to increase the total shear in the time dependent solution, thereby reducing the Richardson number below that of the steady solution. Because these oscillations increase linearly as one moves offshore, the difference between the time dependent and steady Richardson numbers also increases. However, because the oscillatory terms that distinguish the time dependent solution from the steady solution decay with time, the steady solution becomes an increasingly good approximation to the time dependent solution as time progresses. At a fixed position, therefore, the longer it takes the Richardson number to reduce to its critical value, the smaller the difference between the time dependent and steady Richardson numbers. The following section will show that the most important regulating factor in determining how long it takes the Richardson number to reach its critical value is the initial upper layer depth of the system. In Saldanha Bay the appropriate initial upper layer depth is likely to be between 10 and $20m$. Examples of comparisons between time dependent and steady Richardson numbers are given in figures 3.1 to 3.3 for initial upper layer depths of 10 and $20m$. The critical Richardson number has been assumed to have a value of 1, as in the model of Pollard et al (1973). These diagrams indicate that the steady

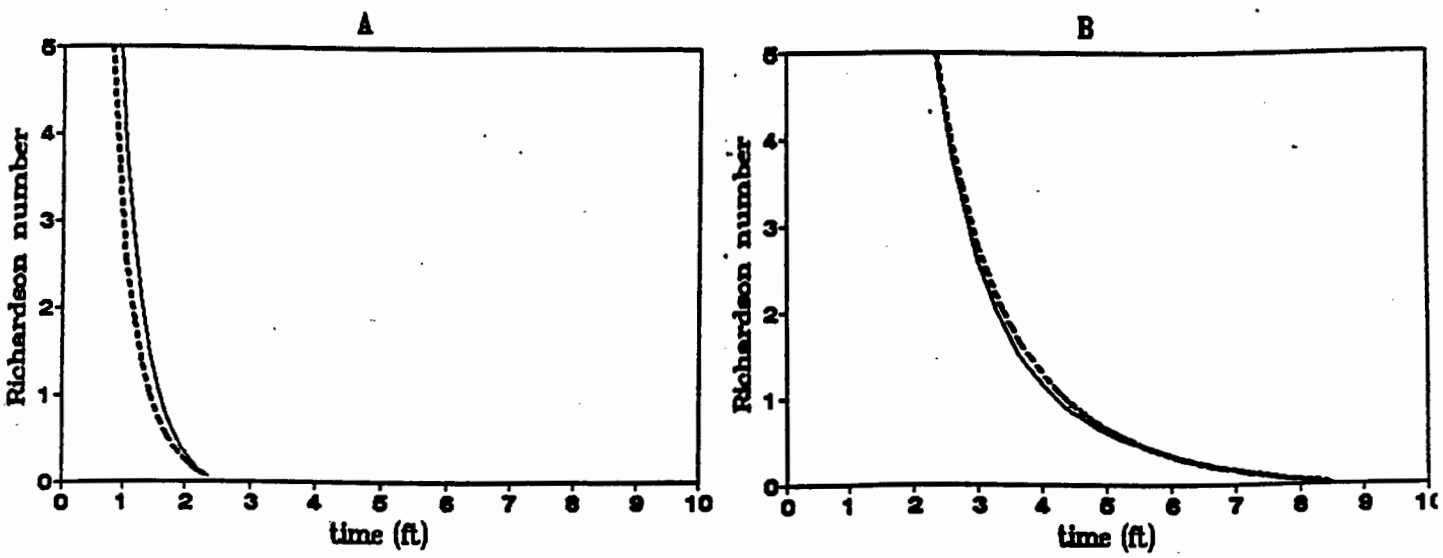

Figure 3.1: Comparisons of the Richardson number for time dependent (solid line) and steady (dashed line) conditions, at the coast ($y = 0$), for an initial upper layer depth of (A)$10m$ and (B)$20m$.

Richardson number has become a useful approximation to the fully time dependent Richardson number by the time that the Richardson number has reduced to its critical value. The steady offshore shear solution for the shear terms and the interface displacement can, therefore, be used to approximate the situation as the Richardson number becomes critical, without introducing unacceptable error. This is equivalent to assuming that the inertial oscillations have died out by the time that the Richardson number has become critical, and can be neglected. Figure 3.3 clearly

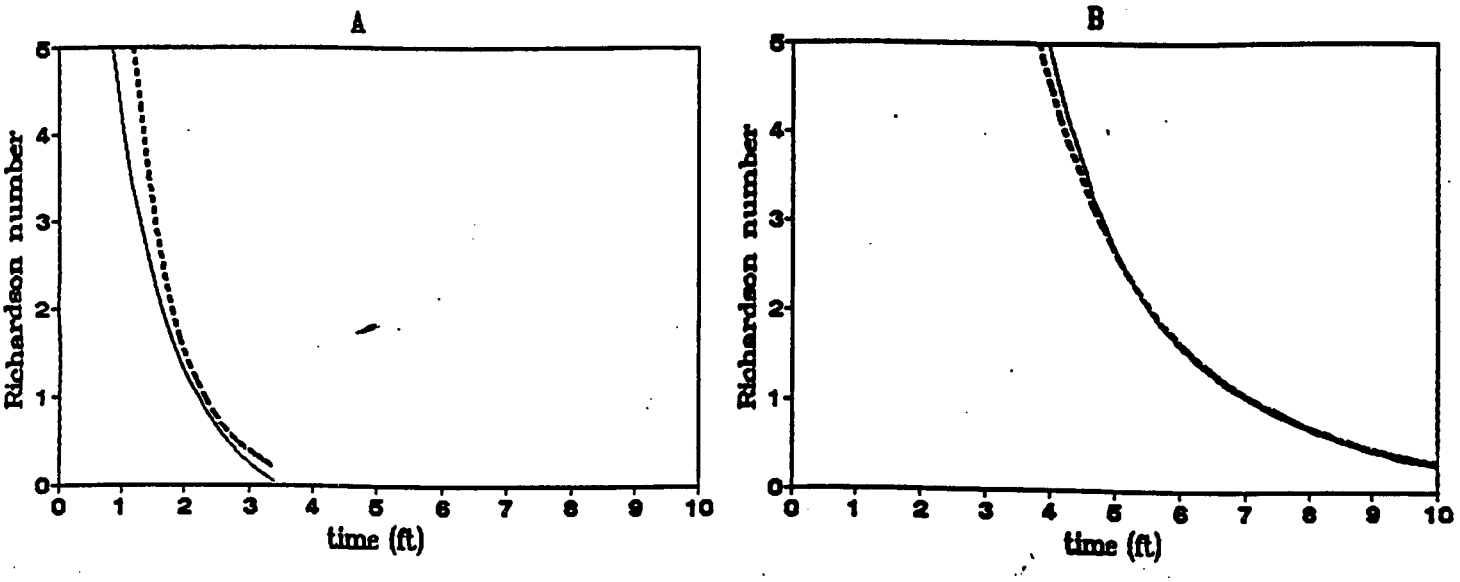

Figure 3.2: Comparisons of the Richardson number for time dependent (solid line) and steady (dashed line) conditions, at half the baroclinic radius offshore ($y = \frac{r_2}{2}$), for an initial upper layer depth of (A)10m and (B)20m.

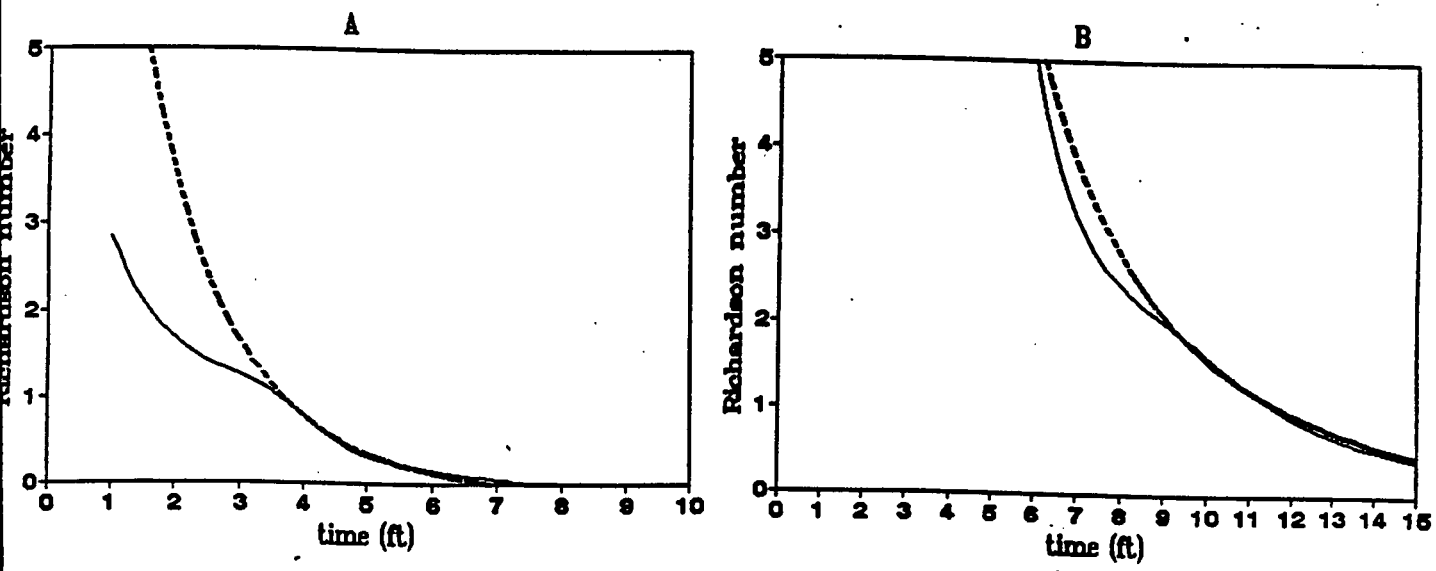

Figure 3.3: Comparisons of the Richardson number for time dependent (solid line) and steady (dashed line) conditions, at the baroclinic radius offshore, for an initial upper layer depth of (A)10m and (B)20m.

reveals the fluctuations in the decline of the time dependent Richardson number that are due to inertial oscillations. These fluctuations are insignificant by the time that the Richardson number has reached its critical value. Another important point that can be gleaned from figures 3.1 to 3.3, is that the Richardson number falls most rapidly at the coast. This means that as the coast is approached, the effects of the enhanced longshore shear and interface displacement outweigh the effects of the reduced offshore shear. The critical value of the Richardson number will be reached at the coast first, and will then slowly move offshore.

3.2 Supercritical Richardson number

Scaling the solutions for steady offshore shear (equations 2.42,2.43 and 2.44), may lead to insights into the behaviour of the system as it approaches the critical Richardson number. Typical scales used in the equations are:

- an offshore length scale R such that $y = Ry_*$, where R is the baroclinic radius ($R \simeq r_2$)
- an interface displacement scale h_1 such that $\epsilon_2 = h_1\epsilon_*$
- a time scale $-\frac{1}{f}$ such that $t = -\frac{1}{f}t_*$

These scales lead to the scaled set of equations, which apply while the Richardson number is greater than its critical value:

$$\epsilon_* = F^{\frac{1}{2}}(\frac{h_2}{H})^{\frac{1}{2}}At_* \tag{3.6}$$

$$Vv_* = \hat{v} = -F^{\frac{1}{2}}(\hat{g}h_1)^{\frac{1}{2}}(1-A) \tag{3.7}$$

$$Uu_* = \hat{u} = -F^{\frac{1}{2}}(\hat{g}h_1)^{\frac{1}{2}}At_* \tag{3.8}$$

Because of the effects of entrainment on longshore shear, it will be a good idea to write the longshore shear in terms of the geostrophic equation (equation 2.34) for future reference.

$$Uu_* = \hat{u} = -(\hat{g}h_1)^{\frac{1}{2}}(\frac{h_2}{H})^{-\frac{1}{2}}(-\frac{\partial\epsilon_*}{\partial y_*}) \tag{3.9}$$

$$= -(\hat{g}h_1)^{\frac{1}{2}}(\frac{h_2}{H})^{-\frac{1}{2}}A\frac{\partial\epsilon_*}{\partial A} \tag{3.10}$$

where

$$A = \exp(-y_*) \tag{3.11}$$

The value of A will vary between 0, an infinite distance from the shore, and 1 at the coast.

The two layer Richardson number is given in equation 3.1. In terms of the scaled terms it will be:

$$Ri = \frac{\hat{g}h_1(1-\epsilon_*)}{(Uu_*)^2+(Vv_*)^2} \tag{3.12}$$

$$= \frac{1-F^{\frac{1}{2}}(\frac{h_2}{H})^{\frac{1}{2}}At_*}{(F^{\frac{1}{2}}At_*)^2+F(1-A)^2} \tag{3.13}$$

This form is appropriate while the Richardson number is greater that its critical value. The offshore shear is steady. The longshore shear and interface displacement, however, will increase with time, decreasing the Richardson number towards its critical value.

If t_{crit} is defined as being the scaled time at which the Richardson number becomes critical, then when the Richardson number becomes critical, equation 3.13 can be written as:

$$Ri_{crit} = \frac{1-F^{\frac{1}{2}}(\frac{h_2}{H})^{\frac{1}{2}}At_{crit}}{(F^{\frac{1}{2}}At_{crit})^2+F(1-A)^2} \tag{3.14}$$

If the critical value of the Richardson number is 1, as in the model of Pollard et al (1973), the positive solution for the time at which the Richardson number becomes critical is:

$$t_{crit} = \frac{-(\frac{h_2}{H})^{\frac{1}{2}}+[\frac{h_2}{H}+4-4F(1-A)^2]^{\frac{1}{2}}}{2F^{\frac{1}{2}}A} \tag{3.15}$$

The length of time it takes for the Richardson number to become critical clearly depends on initial conditions ($\frac{h_2}{H}$ and F) and on position (A). At the coast, $A = 1$, various possibilities for the relative depths of the two layers can be investigated:

- if $h_1 << h_2$ then $\frac{h_2}{H} \simeq 1, t_{crit} \simeq \frac{0.6}{F^{\frac{1}{2}}}$
- if $h_1 \simeq h_2$ then $\frac{h_2}{H} \simeq 0.5, t_{crit} \simeq \frac{0.7}{F^{\frac{1}{2}}}$
- if $h_1 >> h_2$ then $\frac{h_2}{H} \simeq 0, t_{crit} \simeq \frac{1}{F^{\frac{1}{2}}}$

This shows that the important variable in determining the length of time before the Richardson number becomes critical is F, and not $\frac{h_2}{H}$ (see figure 3.4). In any event, $\frac{h_2}{H}$ is always likely to be $\simeq 0.5$ in Saldanha Bay. From equation 3.4 it can be seen that F depends on h_1 to the cubic power, so that the initial upper layer depth assumes more importance than $\hat{g}$ and the wind stress in determining t_{crit}. The shallower the upper layer, the larger the wind stress and the smaller $\hat{g}$, the quicker will the Richardson number reduce to its critical value. Figure 3.4 shows how t_{crit} changes for different values of F. It also shows that the Richardson number becomes critical at the coast first. When the Richardson number becomes critical, entrainment will begin, and figure 3.4 shows that the speed with which the entrainment front moves offshore (given by the slope of the graph) will depend on F. In situations where the initial upper layer depth is large,

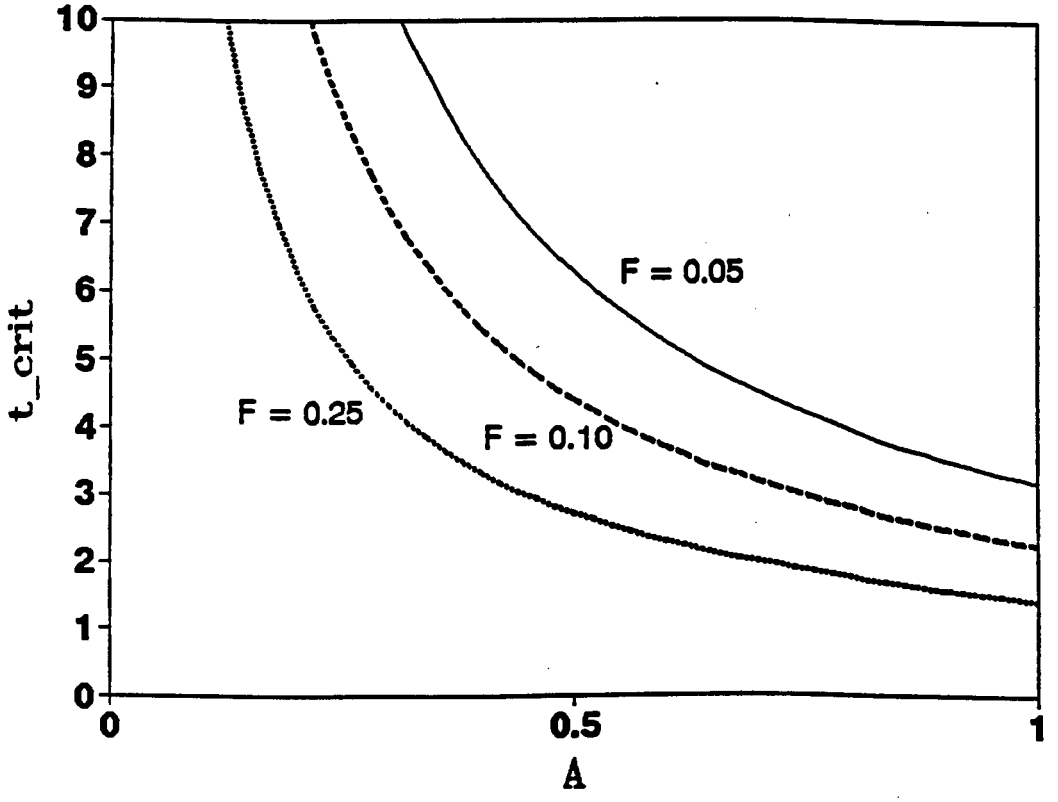

Figure 3.4: Graph showing the relationship between the time that the Richardson number takes to become critical and the offshore distance for three different values of F. The situation shown is for $\frac{h_2}{H} = \frac{1}{2}$.

the approximation that the steady offshore shear solution can be used to investigate entrainment, is a good one. However, if the initial upper layer depth is shallow, inertial oscillations will still be important when entrainment begins.

At t_{crit}, the corresponding position of the scaled interface displacement ϵ_{crit} is given by:

$$\epsilon_{crit} = \frac{-(\frac{h_2}{H}) + (\frac{h_2}{H})^{\frac{1}{2}}[\frac{h_2}{H} + 4 - 4F(1-A)^2]^{\frac{1}{2}}}{2} \tag{3.16}$$

It will be seen later that the slope of t_{crit} is crucial in determining the subsequent entrainment. Because t_{crit} is only a function of A, differentiating t_{crit} with respect to A gives :

$$\frac{dt_{crit}}{dA} = \frac{-4 + 4F(1-A) + (\frac{h_2}{H})^{\frac{1}{2}}[\frac{h_2}{H} + 4 - 4F(1-A)^2]^{\frac{1}{2}} - \frac{h_2}{H}}{2A^2F^{\frac{1}{2}}[\frac{h_2}{H} + 4 - 4F(1-A)^2]^{\frac{1}{2}}} \tag{3.17}$$

Figure 3.4 indicates that the Richardson number will always become critical at the coast first. This means that $\frac{dt_{crit}}{dA}$ is always negative.

3.2.1 critical Richardson number and entrainment

Once the Richardson number becomes critical, entrainment of lower layer water into the upper layer will commence, to ensure that the Richardson number does not become subcritical. If the assumption is made that the entrained water does not significantly change the density of the upper layer, then the offshore shear will not be affected by the entrainment, although the absolute current velocities in each layer will be altered. Once entrainment has begun, the upper layer divergence will be satisfied by a combination of entrainment and further upwelling of the interface, instead of by upwelling of the interface alone. Entrainment must, therefore, reduce the rate of upwelling at all points where the Richardson number is critical. This reduction in the rate of upwelling means that the upwelling equations for the interface displacement (equation 3.6) and longshore shear (equation 3.8) will no longer hold. The assumption that entrainment does not significantly change the density of the upper layer also allows the approximation that the longshore shear is still driven solely by the slope of the interface. The geostrophic equation is thus still valid.

Because the Richardson number becomes critical at the coast first, entrainment will begin there, while the interface is still upwelling at a steady rate further offshore. Entrainment, therefore, causes a change in the shape of the interface. This will affect the longshore shear. Entrainment thus alters the Richardson number both by reducing the rate of interfacial upwelling and by decreasing the longshore shear. In order for the Richardson number to remain critical, a precise combination of entrainment and upwelling must occur. A point to bear in mind is that no matter how much the longshore shear decreases, the offshore shear term remains constant. This implies that there will be a point beyond which the interface cannot upwell, where the mixed layer depth is balanced by the offshore shear term alone. The combination of entrainment and upwelling that

maintains the Richardson number at its critical value must change with time so that entrainment alone will increasingly satisfy the upper layer divergence before this point is reached. A situation where entrainment satisfies the upper layer divergence completely is the maximum amount of entrainment that can occur. In this situation, upwelling of the interface ceases, because there is no longer any surplus upper layer divergence to drive it. This means that the longshore shear must remain constant. Because the offshore shear is always constant, there is nothing that can force the Richardson number to reduce any further. The Richardson number is, therefore, fixed at its critical value. This implies that entrainment cannot subsequently erode the interface to a deeper level.

For $t_* < t_{crit}$ the interface displacement will be given by equation 3.6. A variable, q_*, can be defined as being related to the scaled entrainment length by:

$$entrainmentlength_* = (\frac{h_2}{H})^{\frac{1}{2}} F^{\frac{1}{2}} q_* \tag{3.18}$$

This scaled entrainment length is the entrained volume of water at a point since the Richardson number first became critical at the point. It is an entrainment volume per unit area of interface, and is comparable to the interface displacement. This being so, the interface displacement for $t_{crit} < t_*$ will be:

$$\epsilon_* = \epsilon_{crit} + (\frac{h_2}{H})^{\frac{1}{2}} F^{\frac{1}{2}} [A(t_* - t_{crit}) - q_*] \tag{3.19}$$

where

$$\epsilon_{crit} = (\frac{h_2}{H})^{\frac{1}{2}} F^{\frac{1}{2}} A t_{crit} \tag{3.20}$$

From the preceeding discussion, it is clear that entrainment (and also q_*) is a function of offshore position and the time elapsed since entrainment began. For $t_{crit} < t_*$, the slope of the interface is:

$$\frac{\partial \epsilon_*}{\partial A} = (\frac{h_2}{H})^{\frac{1}{2}} F^{\frac{1}{2}} [t_{crit} + t_* - t_{crit} - (\frac{\partial q_*}{\partial A} - \frac{dt_{crit}}{dA} \frac{\partial q_*}{\partial (t_* - t_{crit})})] \tag{3.21}$$

The longshore shear will assume a different form before and after t_{crit}, because the slope of the interface (on which it depends), is different. Before t_{crit}, the longshore shear is given by equation 3.10, while after t_{crit} the longshore shear is given by:

$$Uu_* = -(\hat{g} h_1)^{\frac{1}{2}} F^{\frac{1}{2}} A [t_{crit} + t_* - t_{crit} - (\frac{\partial q_*}{\partial A} - \frac{dt_{crit}}{dA} \frac{\partial q_*}{\partial (t_* - t_{crit})})] \tag{3.22}$$

The Richardson number before t_{crit} is given by equation 3.13. After t_{crit}, the Richardson number can be obtained by substituting the revised equations for interface displacement and longshore shear into the Richardson number equation (equation 3.12). The result is:

$$Ri = \frac{1 - F^{\frac{1}{2}} (\frac{h_2}{H})^{\frac{1}{2}} A t_{crit} - [F^{\frac{1}{2}} (\frac{h_2}{H})^{\frac{1}{2}} [A(t_* - t_{crit}) - q_*]]}{(F^{\frac{1}{2}} A t_{crit})^2 + F(1 - A)^2 + FA^2 [t_* - \frac{\partial q_*}{\partial A} + \frac{dt_{crit}}{dA} \frac{\partial q_*}{\partial (t_* - t_{crit})}]^2 - (F^{\frac{1}{2}} A t_{crit})^2} \tag{3.23}$$

Examination of this equation indicates that the first two terms in the numerator and the first two terms in the denominator are the same as the Richardson number for $t_* = t_{crit}$ (equation 3.14). In order for the Richardson number to remain critical, the additional terms in the numerator and the denominator must balance. That is:

$$-F^{\frac{1}{2}}(\frac{h_2}{H})^{\frac{1}{2}}[A(t_* - t_{crit}) - q_*] = FA^2[t_* - \frac{\partial q_*}{\partial A} + \frac{dt_{crit}}{dA}\frac{\partial q_*}{\partial(t_* - t_{crit})}]^2 - (F^{\frac{1}{2}}At_{crit})^2 \quad (3.24)$$

Solving for this equation will give the quantity of water entrained. Unfortunately, this equation will be very difficult to solve for. An alternative is to try approximate q_* by looking at some simple constraints.

3.2.2 constraints on entrainment

There are certain basic constraints on the range of values that q_* can take. For instance, if no entrainment takes place anywhere:

$$q_* = 0 \quad (3.25)$$

$$\frac{\partial q_*}{\partial A} = 0 \quad (3.26)$$

$$\frac{\partial q_*}{\partial(t_* - t_{crit})} = 0 \quad (3.27)$$

The interface will continue to upwell at the same rate as before. The numerator of the Richardson number (equation 3.23) will decrease from the critical case, and the denominator will increase. This means that the Richardson number will definitely be less than its critical value. Therefore, in order for the Richardson number to remain critical, entrainment must occur, and $q_* = 0$ provides a minimum constraint on the entrainment that does occur. The other extreme case that can be considered is if the entrainment exactly matches the upper layer divergence, in other words there is no upwelling. In order for this to happen:

$$q_* = A(t_* - t_{crit}) \quad (3.28)$$

$$\frac{\partial q_*}{\partial A} = (t_* - t_{crit}) \quad (3.29)$$

$$\frac{\partial q_*}{\partial(t_* - t_{crit})} = A \quad (3.30)$$

In this case, the numerator of the Richardson number (equation 3.23) will be unchanged, but the denominator will decrease because $\frac{\partial t_{crit}}{\partial A} < 0$ (the Richardson number always becomes critical at the coast first). The Richardson number will, therefore, always be greater than its critical value. A maximum constraint on entrainment is, therefore, that $q_* = A(t_* - t_{crit})$. The value of q_* that maintains the Richardson number at its critical value can be defined as:

$$q_* = q_{crit} \quad (3.31)$$

The simple constraints that have been discussed show that:

$$0 < q_{crit} < A(t_* - t_{crit}) \tag{3.32}$$

These simple constraints can be developed further. Consideration of the Richardson number (equation 3.23), will show that for all values of q_* within the constraints of equation 3.32, the numerator will be smaller than its critical value. If the denominator increases, therefore, the Richardson will have to be less than its critical value. The condition that the denominator of the Richardson number is greater than in the critical case is that:

$$\frac{\partial q_*}{\partial A} - \frac{dt_{crit}}{dA}\frac{\partial q_*}{\partial(t_* - t_{crit})} < t_* - t_{crit} \tag{3.33}$$

Therefore, in order for the Richardson number to remain critical:

$$\frac{\partial q_*}{\partial A} - \frac{dt_{crit}}{dA}\frac{\partial q_*}{\partial(t_* - t_{crit})} > t_* - t_{crit} \tag{3.34}$$

This provides a minimum constraint on the amount of entrainment necessary to maintain the Richardson number at its critical value. It is clearly a more useful minimum constraint than $q_* = 0$. The maximum constraint on entrainment will still be the case of full entrainment and no upwelling. Rewriting this maximum constraint gives:

$$t_* - t_{crit} < \frac{\partial q_{crit}}{\partial A} - \frac{dt_{crit}}{dA}\frac{\partial q_{crit}}{\partial(t_* - t_{crit})} < t_* - t_{crit} - A\frac{dt_{crit}}{dA} \tag{3.35}$$

These constraints suggest that, for large times, entrainment approaches the situation of full entrainment and no upwelling. If the Richardson number became critical at precisely the same time at all positions offshore, entrainment would immediately take its maximum value. However, because the Richardson number becomes critical at the coast first, entrainment is likely to initially occur at a slower rate, and increase towards its maximum value.

The constraints on q_{crit} can be made tighter by considering possible forms for q_*. One possible form for q_* is:

$$q_* = \alpha A(t_* - t_{crit}) \tag{3.36}$$

where α is a constant, so that:

$$\frac{\partial q_*}{\partial A} = \alpha(t_* - t_{crit}) \tag{3.37}$$

$$\frac{\partial q_*}{\partial(t_* - t_{crit})} = \alpha A \tag{3.38}$$

The constraints already discussed have indicated that the rate of entrainment increases with $t_* - t_{crit}$, towards the state of full entrainment and no upwelling. This means that α cannot be

a constant if the Richardson number is to be maintained at its critical value. Regarding α as a constant may, however, enable time-dependent constraints to be placed on the value of q_{crit}. In this form, $\alpha = 0$ corresponds to a situation where no entrainment takes place after t_{crit}, and the interface continues to upwell at the same rate as before. If $\alpha = 1$, entrainment completely satisfies the upper layer divergence, and the interface no longer upwells. Substituting for q_* in the Richardson number (equation 3.23) will give:

$$Ri = \frac{1 - F^{\frac{1}{2}}(\frac{h_2}{H})^{\frac{1}{2}} A t_{crit} - [F^{\frac{1}{2}}(\frac{h_2}{H})^{\frac{1}{2}} A(t_* - t_{crit})(1-\alpha)]}{(F^{\frac{1}{2}} A t_{crit})^2 + F(1-A)^2 + FA^2[t_* - \alpha(t_* - t_{crit}) + \alpha A \frac{dt_{crit}}{dA}]^2 - (F^{\frac{1}{2}} A t_{crit})^2} \quad (3.39)$$

At a particular position (A) and time after entrainment has begun ($t_* - t_{crit}$), a value of α can be numerically determined that will ensure that the Richardson number is greater than critical. This can be achieved by repeatedly calculating the Richardson number for various values of α, until a value of α is found for which the Richardson number is marginally supercritical. Because the rate of entrainment appears to increase with time, this value of α will also produce supercritical Richardson numbers at all earlier times. The q_* corresponding to this value of α (obtained through equation 3.36), reflects the minimum entrainment that will ensure a supercritical Richardson number. Therefore, in order for the critical Richardson number to be maintained, this value of q_* must represent a maximum constraint on q_{crit}. Unfortunately, a minimum constraint cannot be determined in the same way. A value of α that produces a Richardson number that is smaller than the critical value at a particular time, will not necessarily produce a subcritical Richardson number at earlier times. A minimum constraint based on α would, therefore, be inconsistent.

In an attempt to find a minimum constraint, a different form for q_* needs to be considered. Because the rate of entrainment appears to be a function of the time elapsed since the Richardson number first became critical, a suitable form for q_* may be:

$$q_* = \beta A(t_* - t_{crit})^2 \quad (3.40)$$

where β is a constant, so that:

$$\frac{\partial q_*}{\partial A} = \beta(t_* - t_{crit})^2 \quad (3.41)$$

$$\frac{\partial q_*}{\partial t_* - t_{crit}} = 2\beta A(t_* - t_{crit}) \quad (3.42)$$

This form for q_* has the advantage that the rate of entrainment is initially zero, but thereafter increases with time. The situation where no entrainment occurs after t_{crit} corresponds to $\beta = 0$. Substituting into the Richardson number (equation 3.23) for q_* gives:

$$Ri = \frac{1 - F^{\frac{1}{2}}(\frac{h_2}{H})^{\frac{1}{2}} A t_{crit} - [F^{\frac{1}{2}}(\frac{h_2}{H})^{\frac{1}{2}} A(t_* - t_{crit})(1 - \beta[t_* - t_{crit}])]}{F(1-A)^2 + FA^2[t_* - \beta(t_* - t_{crit})^2 + 2\beta A(t_* - t_{crit})\frac{dt_{crit}}{dA}]^2} \quad (3.43)$$

A value of β can now be numerically determined (for a particular A and $t_* - t_{crit}$) for which the Richardson number is marginally less than critical. At all earlier times, this value of β will result in Richardson numbers that are less than critical. The corresponding value of q_* (obtained through equation 3.40), refects the maximum entrainment that can occur at that time, while ensuring that the Richardson number is less than its critical value. In order for the critical Richardson number to be maintained, entrainment must be greater than this amount, with q_* consequently representing a minimum constraint on q_{crit}.

The numerical constraints on q_{crit} can be determined with a simple computer program. At a particular time, these minimum and maximum constraints can be calculated to any desired level of accuracy, effectively producing an approximation to q_{crit} at this time. If this procedure is repeated for different times, the evolution of entrainment over time becomes apparent. Figure 3.5 displays a representative graph of the approximation of q_{crit} evaluated at a particular point. This q_{crit} is related to the scaled entrainment length through equation 3.18. It enables the calculation of the quantity of water entrained at a point since the Richardson number first became critical (t_{crit}). Once q_{crit} is known, the position of the interface at the corresponding time can be determined from equation 3.19. Knowledge of the approximate quantity of water entrained into the upper layer while a steady wind is blowing can be used to determine the nutrient and heat flux from the lower layer to the upper layer. This is important information in the determination of simple nutrient and heat budgets for Saldanha Bay.

3.3 Simple budgets

In winter there is only an upper layer in Saldanha Bay. The upwelling-favourable winds during summer, however, cause a tongue of cold water to be drawn into the bay, effectively separating the bay into two vertical layers. The winds associated with the upwelling cause an offshore volume flux in the upper layer, which is the steady Ekman volume flux response to the wind. At any point offshore, the spatial gradient of the Ekman flux must be balanced by an upward volume flux. The upward volume flux consists of an upwelling component ($Uflux$) and an entrainment component ($Eflux$). The upwelling component is associated with a shoaling of the interface separating the layers, while the entrainment component consists of water moving across the interface from the lower layer into the upper layer. Because entrainment only begins after a particular time (t_{crit}), the upwelling flux is initially steady, and equal to the gradient of the Ekman flux. After t_{crit}, however, the gradient of the Ekman flux at a point will be equal to the sum of the upwelling and entrainment fluxes. The entrainment flux must, therefore, cause a reduction in the upwelling flux from its steady value. The volume budget of the upper layer thus consists of a volume efflux that is equal to the spatial gradient of the Ekman flux, and an influx of volume equal to the entrainment flux. Because the Ekman flux is always larger than the entrainment flux, the volume of the upper layer must decrease with time.

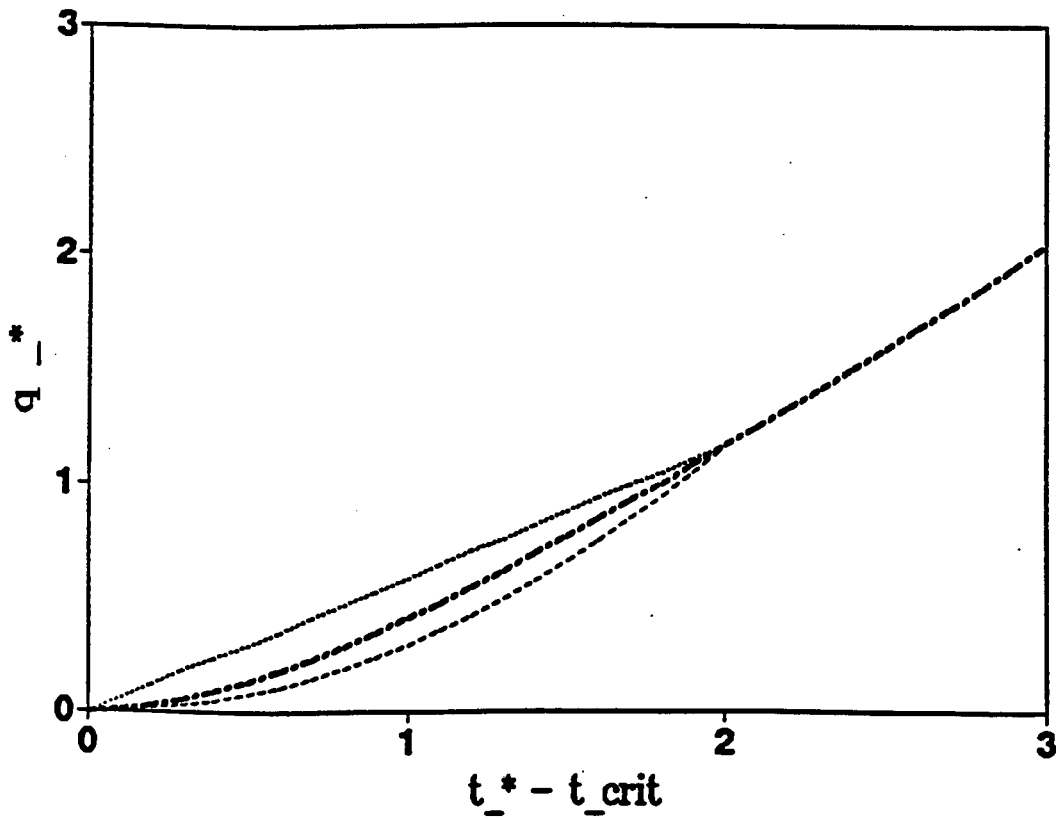

Figure 3.5: Graph showing q_* versus $t_* - t_{crit}$ for the case at the coast, with $F = 0.1$ and $\frac{h_2}{H} = 0.5$. The bold dashed line represents the approximate value of q_{crit}. The lighter dotted line is the maximum constraint on q_* evaluated at $t_* - t_{crit} = 2$. All points above this line lie in a region where $Ri > 1$, but nothing can be said about the points that lie below the line. The light dashed line is the minimum constraint on q_* evaluated at $t_* - t_{crit} = 2$. All points below this line lie in the region where $Ri < 1$, although nothing can be said about the points that lie above the line. At the time that the constraints are evaluated, the feasible region for $Ri = 1$ is small enough for q_{crit} to be approximated.

The entrainment flux is capable of injecting properties of the lower layer water into the upper layer. The change in a water property in the upper layer will equal the inflow of that water property into the upper layer, less the flow of that property out of the upper layer. As has already been noted, entrainment is a one-way process, which means that water properties cannot flow from the upper to lower layers. In order to keep the upper layer nutrient and heat budgets as simple as possible, the assumption will be made that the water properties in the upper layer are always homogenous, and that the properties in the lower layer are fixed.

3.3.1 a simple nutrient budget

In the upper layer of Saldanha Bay, the only natural input of nutrients will be through the entrainment flux of nutrient-rich lower layer water. The upwelling flux does not introduce nutrients, because it does not represent a flux of water across the interface. The injection of the nutrients into the upper layer will stimulate biological productivity, and this uptake of nutrients by phytoplankton will represent a "flow" of nutrients out of the upper layer. A very simple nutrient budget can be derived if the assumption is made that the concentration of nutrients in the upper layer is negligible compared to the nutrient concentration in the lower layer. This is equivalent to assuming that biological productivity instantaneously adjusts to fully capitalise on all available upper layer nutrients. Implicit in this assumption is that productivity in the system is nutrient limited.

$$nutrient_1(t+\Delta t) = nutrient_1(t) + nutrientflux.\Delta t - uptakerate.\Delta t \quad (3.44)$$

$$\frac{dnutrient_1}{dt} = nutrientflux - uptakerate \quad (3.45)$$

Noting that:

$$nutrient_1 = conc_1.H_1(t) \quad (3.46)$$

$$\frac{dH_1}{dt} = -Uflux \quad (3.47)$$

$$nutrientflux = Eflux.[conc_2 - conc_1(t)] - Uflux.conc_1(t). \quad (3.48)$$

where $conc_1(t)$ denotes the time dependent upper layer nutrient concentration
$conc_2$ denotes the steady lower layer nutrient concentration
and $H_1(t)$ is the time dependent depth of the upper layer

Substitution for these variables results in the dependence on $Uflux$ being removed, and enables equation 3.45 to be rewritten as:

$$\frac{dconc_1.}{dt} = \frac{Eflux}{H_1(t)}[conc_2 - conc_1(t)] - \frac{uptakerate}{H_1(t)} \quad (3.49)$$

The preceding discussion has indicated that a simple budget can be derived if the nutrient concentration in the upper layer is always negligible. In this case, the amount of nutrient in the upper layer is approximately constant and zero, so that:

$$uptakerate = conc_2.Eflux \tag{3.50}$$

Estimates of the entrainment velocity thus allow estimates to be made of the nutrient uptake rate.

3.3.2 a simple heat budget

A simple heat budget for the upper layer can be derived in much the same way as the nutrient budget. There will, however, be two separate fluxes of heat into the upper layer, that due to entrainment and that due to the surface heat flux.

$$heat_1(t+\Delta t) = heat_1(t) + heatflux.\Delta t \tag{3.51}$$

$$\frac{dheat_1}{dt} = heatflux \tag{3.52}$$

Noting that:

$$heat_1 = Cp.\rho.T_1(t).H_1(t) \tag{3.53}$$

$$\frac{dH_1}{dt} = -Uflux \tag{3.54}$$

$$heatflux = Cp.\rho.Eflux.[T_2 - T_1(t)] - Cp.\rho.T_1(t).Uflux + Q \tag{3.55}$$

where Q is the surface heat flux
Cp is the heat capacity of water ($4180 J.kg^{-1}.K^{-1}$)
T is the absolute temperature of the water

Substituting for these variables allows equation 3.52 to be rewritten as:

$$\frac{dT_1}{dt} = \frac{Eflux}{H_1(t)}.[T_2 - T_1(t)] + \frac{Q}{Cp.\rho.H_1(t)} \tag{3.56}$$

The first term on the right hand side is the heat flux due to entrainment of water from the lower layer. The variable $T_1(t)$ represents the past history of entrainment and surface heating inshore of the point. Because $T_1(t) > T_2$, entrainment will tend to decrease the temperature of the upper layer. In the vicinity of Saldanha Bay, the daily averaged surface heat flux is always likely to be positive, so that the effects of entrainment and surface heating will tend to counteract one another. Whether the upper layer temperature increases or decreases, will depend on which term is larger. Of course, the changes in the upper layer temperature, and thus in density, are neglected in the model of entrainment. The entrainment model, therefore, implicitly assumes that the entrainment heat flux and surface heat flux terms sum to zero. This means that the feedback loop between upper layer temperature and entrainment has not been considered.

3.4 Summary

This chapter has investigated coastal entrainment. The first section is devoted to showing that inertial oscillations have little effect on entrainment, if the initial upper layer depth is reasonably large. This allowed the shear and interface displacement solutions for the model of steady offshore shear, introduced in the previous chapter, to be scaled and used to investigate the situation leading up to the Richardson number becoming critical. The time taken for the Richardson number to become critical was determined, and was found to be highly dependent on the initial upper layer depth. It was also found to be dependent on the offshore position, with the Richardson number first becoming critical at the coast, and subsequently becoming critical further offshore. Once the Richardson number becomes critical, entrainment acts to ensure that the Richardson number does not become subcritical.

Throughout the subsequent work the assumption was made that entrainment would not affect the density of the upper layer. This assumption will clearly be a poor one if large quantities of water are entrained into the upper layer. A consequence of this assumption is that the offshore shear remains constant, although the absolute velocities in both layers will be altered by entrainment. Any entrainment that occurs will reduce the upwelling of the interface, because the upper layer divergence at that point is now satisfied by both entrainment and upwelling. Entrainment will begin at the coast, while further offshore the Richardson number will still be supercritical and upwelling of the interface will continue steadily. This leads to a change in the shape of the interface, which will reduce the longshore shear from its value when the Richardson number first became critical. This impact of upwelling on the longshore shear complicates the dynamics, as entrainment and upwelling of the interface (which are interacting) are forced to proceed at a rate that maintains the critical Richardson number. An equation for the entrainment is derived, but it is hard to see how it could be solved simply. Instead, constraints on the minimum and maximum amounts of entrainment that can occur are investigated. Clearly the maximum amount of entrainment that can ever occur is such that entrainment alone satisfies the upper layer divergence, and no upwelling occurs. Because no upwelling occurs, the position of the interface is fixed, which prevents the longshore shear from changing. As long as the offshore shear is assumed to be constant, the Richardson number will remain at its critical value. There is, therefore, nothing that can reduce the Richardson number further, and so entrainment will remain at this level. The minimum and maximum constraints on entrainment can be made suitably close together by numerically calculating the Richardson number. These constraints suggest that the actual amount of entrainment that occurs increases with time, until a situation is reached where entrainment is satisfying all the upper layer divergence.

The final section of this chapter shows how the estimates of entrainment can be used to supply vital information in simple budgets of heat and nutrients in the upper layer. The nutrient budget

will enable an estimate to be made of the uptake of nutrients by phytoplankton in the upper layer. The heat budget, meanwhile, will provide an indication of the validity of the assumption, made in the model of coastal entrainment, that the upper layer temperature remains steady. Later, this heat budget will also be used to ascertain the appropriate area over which the model should be applied in Saldanha Bay.

Chapter 4

RESULTS

This chapter will be divided into three main sections. The first section looks at the behaviour of entrainment, through equations 3.18,3.19,3.36,3.39,3.40 and 3.43, near a coast, if typical wind stress and stratification conditions prevail. The second section shows how the strength and duration of synoptic events can affect the amount of water entrained by the upper layer, while the third section examines the effects of these synoptic events on the upper layer nutrient and heat budgets.

4.1 A typical wind event

The aim of this section is to display the nature of the entrainment process near the coastal boundary during a typical wind event. This typical wind event will have a value of F equal to 0.1. Important variables to be considered are the interface displacement, the volume of water entrained into the upper layer, and the rate at which this water is entrained. All the variables are scaled, the actual quantities can easily be determined by examining the appropriate scales in the previous chapter.

Figures 4.1 and 4.2 display the variation of the scaled interface depth with scaled time and offshore distance respectively. The time scale chosen extends from $t_* = 0$ (when the wind starts blowing) to $t_* \simeq 6\pi$ (which is approximately three days later). The length scale extends from the coast at $y_* = 0$ to $y_* = 2$, which is a point two baroclinic radii from the coast. This point was chosen as a limit, because this thesis is concerned with the entrainment that occurs adjacent to the coast. An important point to bear in mind is that the position of the interface is only altered by upwelling. The distance from the top of the figure to the graph can be viewed as the scaled depth of the upper layer, and it can clearly be seen that this depth decreases with time and proximity to the coast. These graphs indicate that there are three stages during a typical wind event. The first stage is characterized by the interface displacement increasing linearly with time. At the same time, the interface will slope away from the coast exponentially, indicating

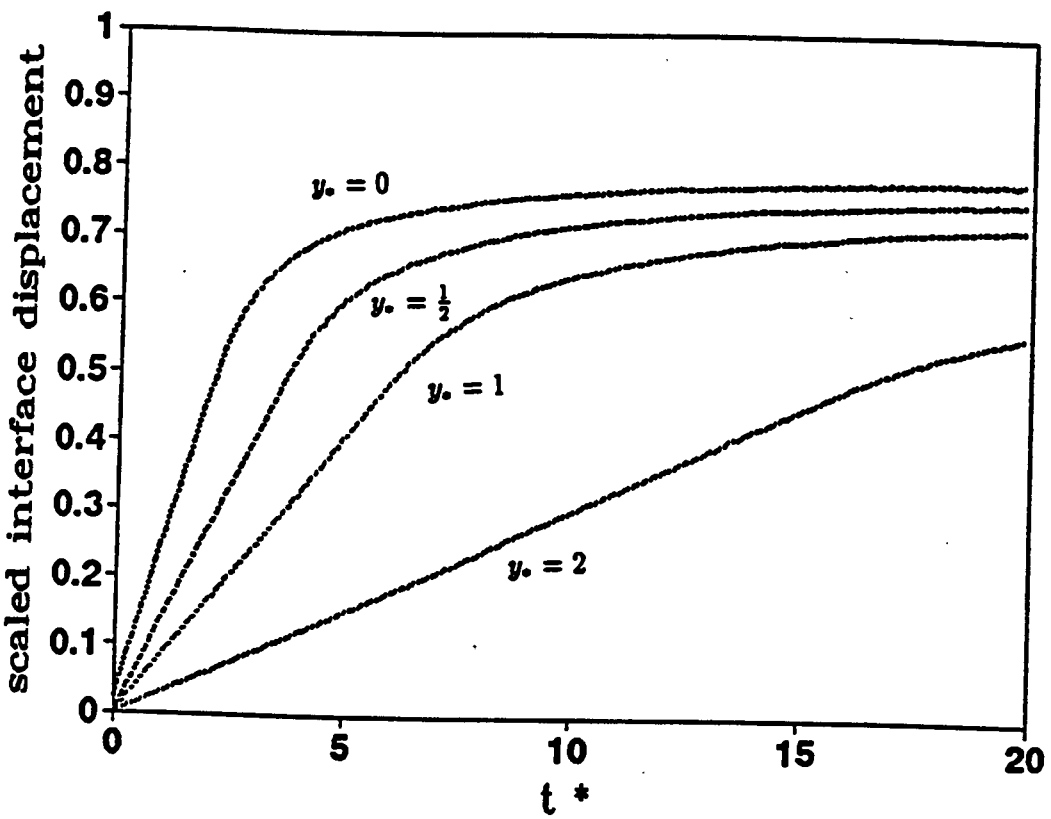

Figure 4.1: Graph illustrating the variation of the scaled interface displacement with time when $F = 0.1$. The interface displacement is shown at the coast, and at points half a baroclinic radius offshore, one radius offshore, and two radii offshore. The time scale extends from $t_* = 0$ (when the wind first begins blowing) to $t_* = 20$ (which is approximately three days later).

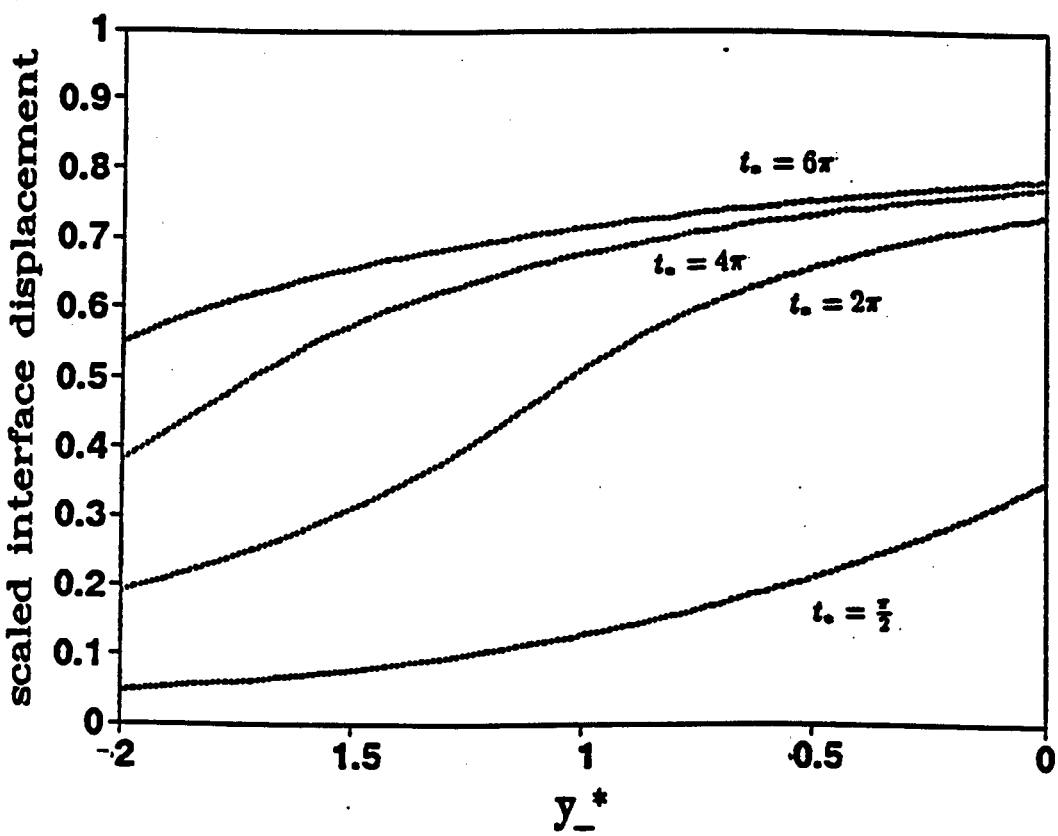

Figure 4.2: Graph illustrating the variation of the scaled interface displacement with offshore distance when $F = 0.1$. The situation is depicted at $t_* = \frac{\pi}{2}$, $t_* = 2\pi$, $t_* = 4\pi$, and $t_* = 6\pi$. The offshore scale extends from the coast to a point two baroclinic radii offshore.

that the steady upwelling flux decreases exponentially away from the coast. The previous chapters have established that the interface will upwell steadily from the time that the wind stress is switched on until the Richardson number has reached its critical value (t_{crit}), and that this critical value will be reached at the coast first. Figure 4.1 indicates that this stage lasts for $t_* \simeq 2$ at the coast, and for $t_* \simeq 16$ at a point twice the baroclinic radius offshore. Once the Richardson number has reached its critical value, entrainment will begin, which will reduce the upwelling rate. This second stage is an adjustment stage, where the interface upwells at a decreasing rate, because entrainment is satisfying an increasing percentage of the divergence in the upper layer. Because entrainment first begins at the coast, there will be a time delay between the second stage commencing at the coast and at points further offshore. This will cause the reduction in the rate of upwelling to vary in the offshore direction. The offshore slope of the interface will thus be altered from its exponential shape, as upwelling slows near the coast but remains constant further offshore. By the end of this stage, the upwelling rate is small, and the position of the interface has become approximately constant with time. The third stage, where the entrainment has become fully realised, is characterized by a constant interface displacement, and an upper layer of fixed depth. An important point to note is that the interface displacement does not reach a value of 1, indicating that entrainment prevents the interface from reaching the surface. Once the third stage has been reached, figure 4.2 indicates that the exponential offshore interface slope of stage one will have been replaced by a small linear interface slope. This implies that the adjustment process significantly reduces the longshore shear from its value when entrainment first begins.

The three stages are also apparent in figures 4.3 and 4.4. These diagrams show the variation in the flux of water entrained into the upper layer with time and offshore position respectively. The first stage is characterized by no entrainment, and there is thus no flux of water into the upper layer. The second stage begins at t_{crit}, which is the point where the graphs in figure 4.3 intersect the X-axis. The offshore variation in the time taken before the commencement of this stage can clearly be seen. During the second stage, the entrainment flux increases from a value of zero towards a value that would completely satisfy the divergence in the upper layer. The entrainment flux effectively replaces the upwelling flux. During the first stage, the steady upwelling flux completely satisfies the upper layer divergence. The original upwelling flux will, therefore, represent an asymptote which imposes a maximum limit on the entrainment flux. This asymptote has a value of $F^{\frac{1}{2}}(\frac{h_2}{H})^{\frac{1}{2}}A$. As the entrainment flux approaches this asymptote, it will become approximately constant in time, which characterizes the third stage. The form of the asymptote indicates that the entrainment flux will decrease in an exponential fashion away from the coast, in the third stage. In other words the entrainment flux in the third stage will vary with offshore position in the same way as the upwelling flux does in the first stage. The graphs in figure 4.4 do not display a true exponential relationship, because they depict a combination of the second and third stages. The offshore sections of the graphs display the entrainment flux that characterizes the second stage. At early times, much of the displayed graph falls into this second stage, and the

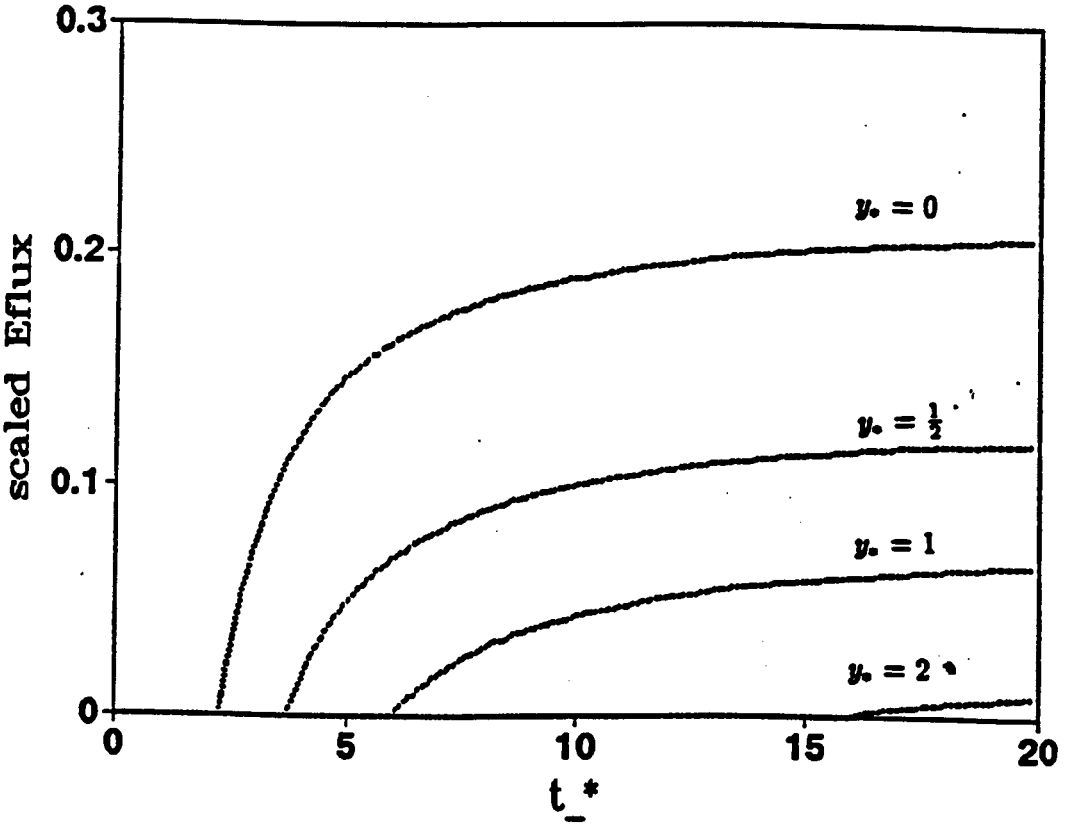

Figure 4.3: Graph illustrating the variation of the scaled entrainment flux with time when $F = 0.1$. The flux is shown at the coast, and at points half a baroclinic radius offshore, one radius offshore, and two radii offshore. The time scale extends from $t_* = 0$ (when the wind first begins blowing) to $t_* = 20$ (which is approximately three days later).

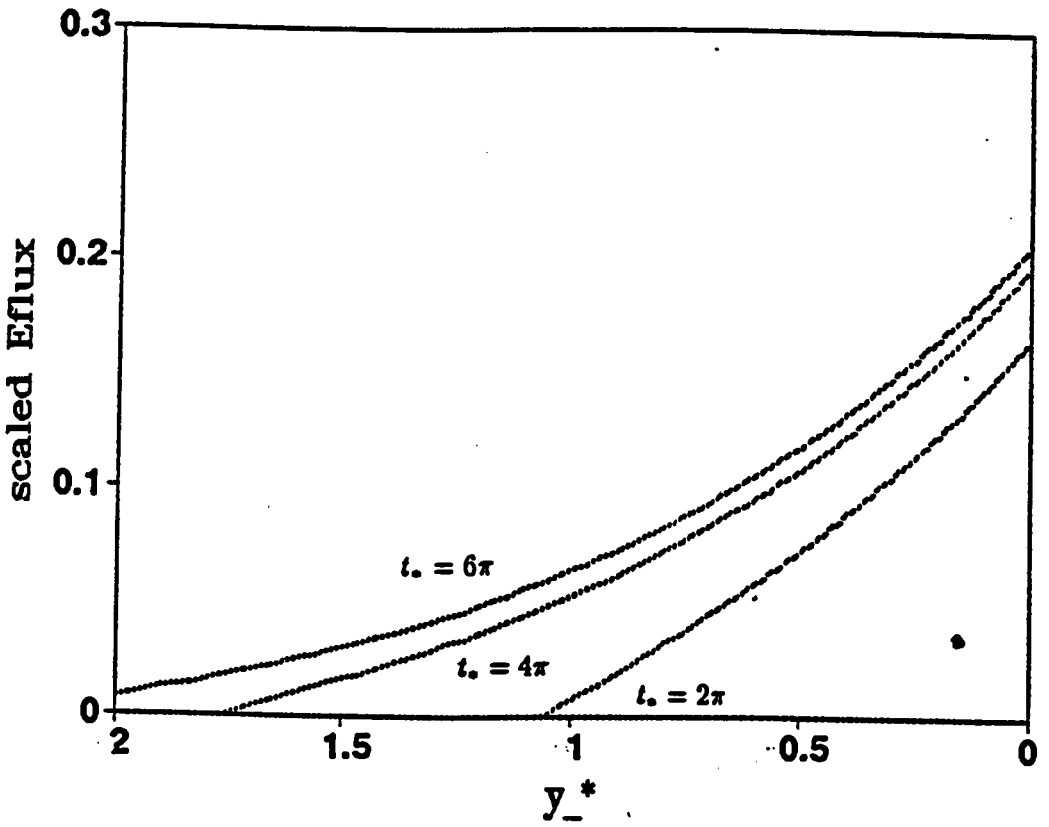

Figure 4.4: Graph illustrating the variation of the scaled entrainment flux with offshore distance when $F = 0.1$. The situation is depicted at $t_* = 2\pi$, $t_* = 4\pi$, and $t_* = 6\pi$. The offshore scale extends from the coast to a point two baroclinic radii offshore.

entrainment flux appears to decrease linearly away from the coast. As time progresses, however, more of the displayed graph falls into the third stage, and the entrainment flux decreases in a near-exponential fashion away from the coast.

Figures 4.5 and 4.6 illustrate the variation of the entrainment length with time and offshore position respectively. This entrainment length is a time integrated entrainment flux. The graphs in figure 4.5 give, therefore, the total volume of water entrained into the upper layer, per unit area. Integrating the graphs in figure 4.6 will give the total volume of water entrained into the upper layer, per unit length of coastline. Because they are essentially an integrated version of figures 4.3 and 4.4, figures 4.5 and 4.6 convey much the same information. The first stage, where there is only upwelling and no entrainment, ends where the graphs intersect the X-axis in figure 4.5. The suggestion of curvature, as the graphs rise from the X-axis, signifies the increasing entrainment flux that characterizes the second stage, while the near-linear portion of the graph that follows is due to the near-steady entrainment flux of the third stage. Figure 4.6 indicates that the entrainment length decreases in a linear fashion for small times, but that it decreases in a near-exponential fashion for larger times. This is consistent with the graphs in figure 4.4.

4.2 Comparison of wind events

The variation of the entrainment process with time and offshore distance has been demonstrated, for a typical event, in the previous section. This basic picture should remain unchanged for all events for which the model is valid, that is for $0 < F < 0.25$. It will be of interest, however, to examine the effect of the strength of a wind event on entrainment and the nutrient and heat budgets. In order to achieve this it will be assumed that:

- the initial upper layer depth (h_1) is $15m$
- the total water depth (H) is $30m$
- the upper layer density (ρ_1) is $1024kg.m^{-3}$
- the lower layer density (ρ_2) is $1026kg.m^{-3}$
- the latitude is $33°S$

The density difference between the two layers corresponds to a temperature difference of $8°C$. Strong, fresh and moderate wind events will be considered. The strong wind event will blow at $13.4m.s^{-1}$ ($F \simeq 0.213$), the fresh event at $9.3m.s^{-1}$ ($F \simeq 0.038$), and the moderate event at $6.2m.s^{-1}$ ($F \simeq 0.008$). These wind events were selected to correspond to force 6, 5 and 4 events respectively on the Beaufort Scale, and represent a typical range of wind speeds in the Saldanha Bay region.

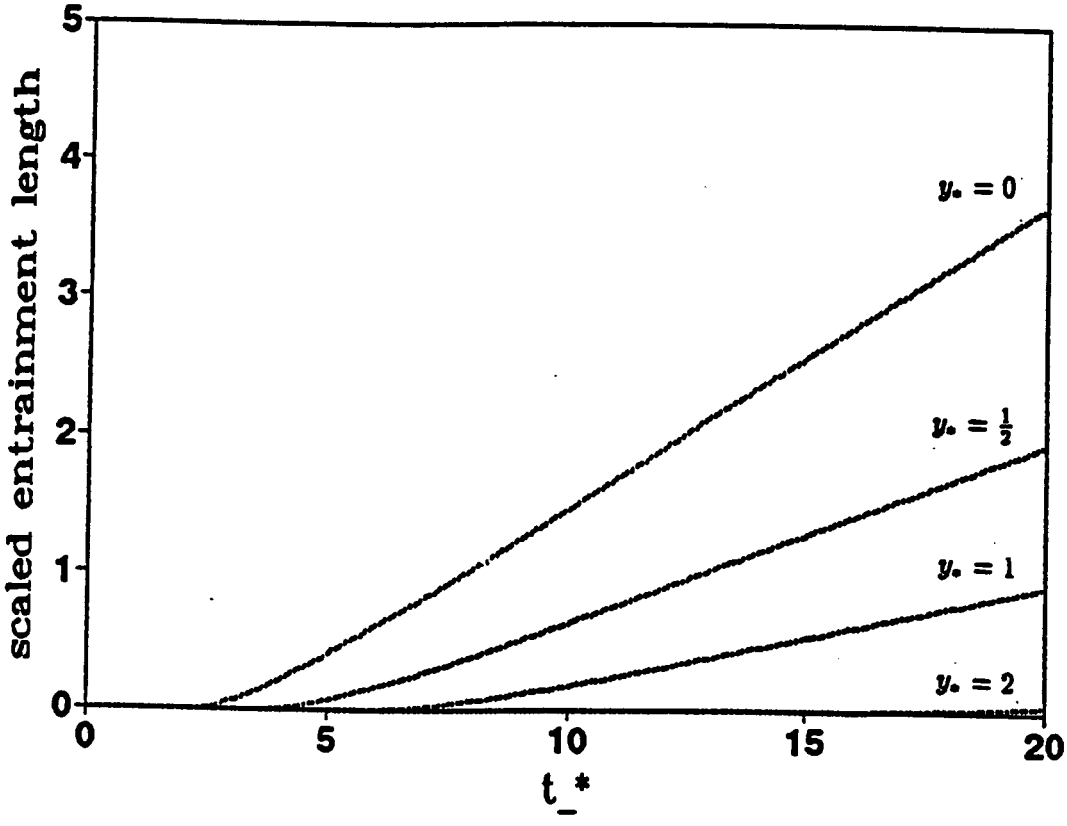

Figure 4.5: Graph illustrating the variation of the scaled entrainment length with time when $F = 0.1$. The length is shown at the coast, and at points half a baroclinic radius offshore, one radius offshore, and two radii offshore. The time scale extends from $t_* = 0$ (when the wind first begins blowing) to $t_* = 20$ (which is approximately three days later).

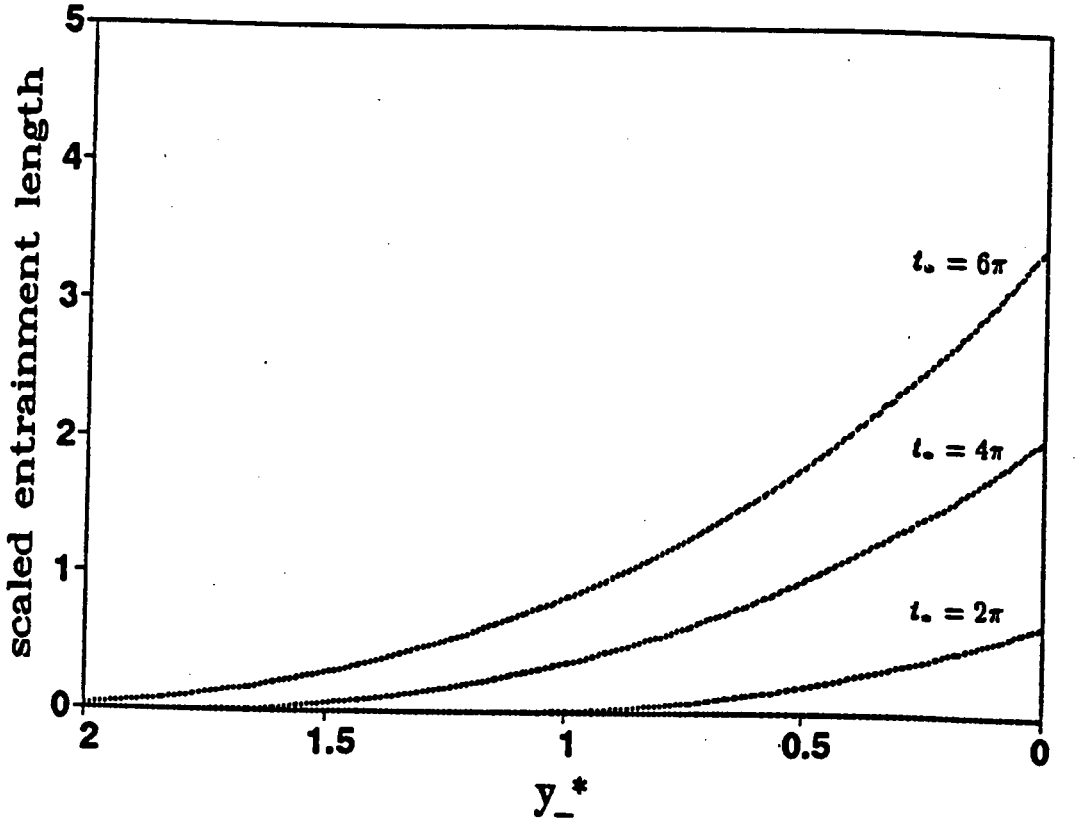

Figure 4.6: Graph illustrating the variation of the scaled entrainment length with offshore distance when $F = 0.1$. The situation is depicted at $t_* = 2\pi$, $t_* = 4\pi$, and $t_* = 6\pi$. The offshore scale extends from the coast to a point two baroclinic radii offshore.

Wind speed is related to wind stress by the well known relationship:

$$X_s = C_D \rho_a {u_{10}}^2 \tag{4.1}$$

where ρ_a is the density of air (~ 1.2)
where u_{10} is the wind speed at a height of 10 metres
and where C_D is a drag coefficient
The value of this drag coefficient is approximately given by Large and Pond (1981):

$$\begin{aligned} C_D &= 1.2 && \text{for } 4 \leq u_{10} \leq 11 \\ &= 0.49 + 0.065 u_{10} && \text{for } 11 \leq u_{10} \leq 25 \end{aligned} \tag{4.2}$$

Each wind event will last for $t_* = 6\pi$ (approximately three days), which is probably the maximum duration over which the wind stress can reasonably be assumed to be steady. Because the offshore variation in entrainment is likely to be similar in all these cases to that of the typical event presented in the previous section, only the situation at the coast will be considered.

Figure 4.7 shows the variation in the depth of the interface with time for the three different wind events. The figure reveals the same pattern at the coast as was demonstrated for a typical wind event in the previous section. As would be expected, the interface shoals more rapidly (in stage two) during the stronger wind events. An interesting result, however, is that the position at which the interface becomes approximately constant (in stage three), is quite similar for the wind events that have been considered. The depth of the upper layer in stage three is not, therefore, very sensitive to the strength of the wind event. Another important point is that strong wind events are associated with shallower surface mixed layers than weak wind events. This is the opposite to what would be expected in the open ocean, where strong wind events result in deeper surface mixed layers than weak wind events.

The variation in the entrainment length with time, at the coast, is illustrated in figure 4.8. It is important to remember that these graphs represent the volume of water, per square metre, entrained at the coast since the wind event began. The graphs clearly show that it takes longer for entrainment to occur under a weak wind regime than under a strong one. The graphs also demonstrate that there is dramatically more entrainment during strong wind events than during weak events. This point is not obvious from the graphs of interface displacement presented in figure 4.7. The position of the interface is, therefore, a poor diagnostic for the amount of entrainment that takes place.

Another interesting comparison that can readily be made, is to compare the entrainment that occurs in events which have the same time-integrated wind stress. Figure 4.9 depicts the variation of the scaled entrainment flux with time, at the coast. Three different scenarios are shown, all

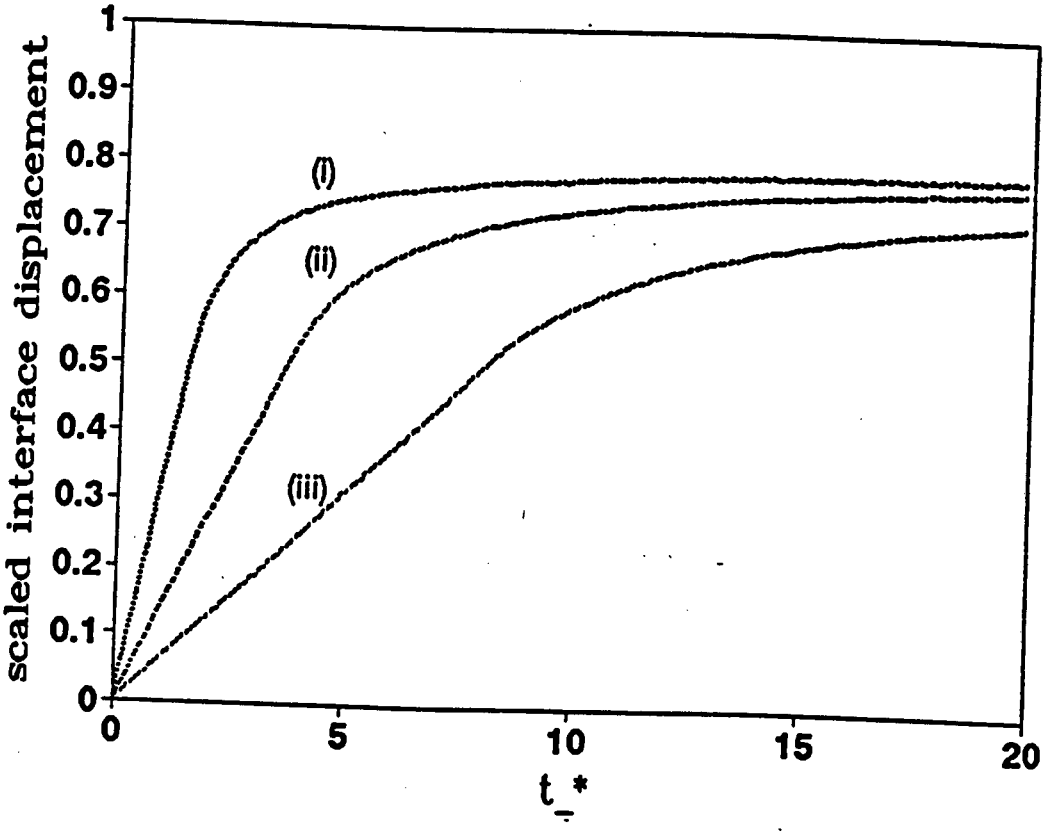

Figure 4.7: Graph depicting the variation in the scaled interface displacement with time for a wind event of (*i*) $13.4m.s^{-1}$, (*ii*) $9.3m.s^{-1}$, and (*iii*) $6.2m.s^{-1}$. The respective values of F are 0.213, 0.038 and 0.008.

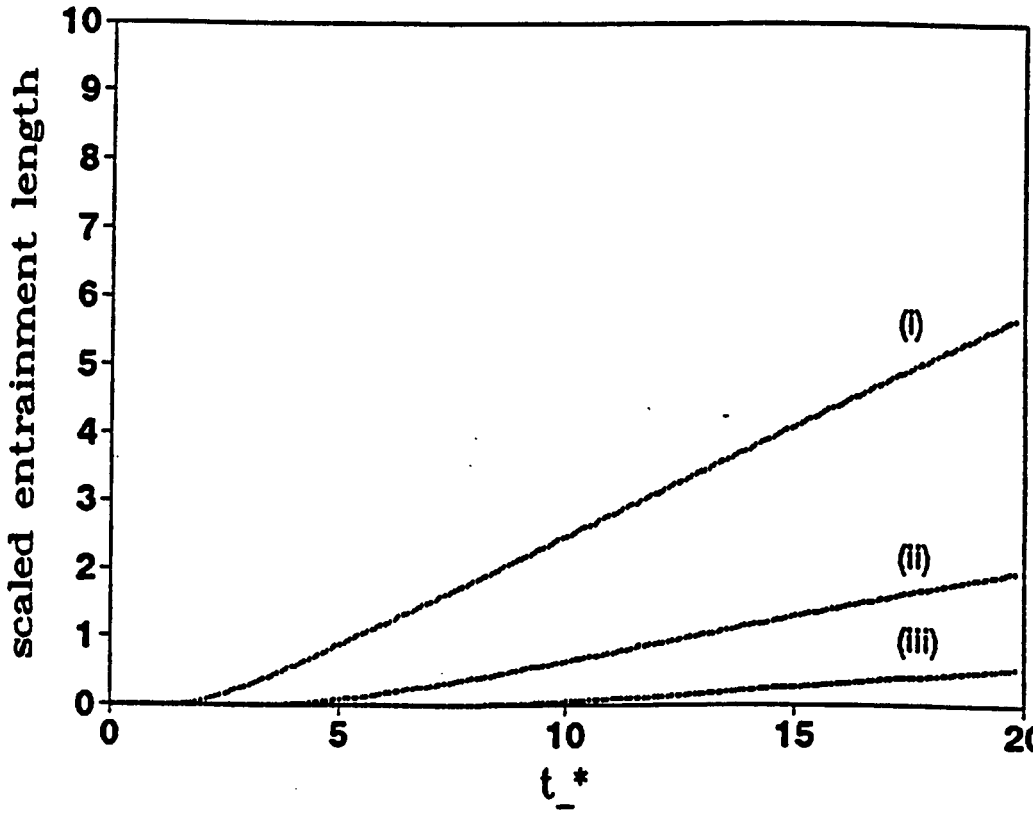

Figure 4.8: Graph depicting the variation in the scaled entrainment length with time for a wind event of (i) $13.4m.s^{-1}$, (ii) $9.3m.s^{-1}$, and (iii) $6.2m.s^{-1}$. The respective values of F are 0.213, 0.038 and 0.008.

of which have the same time-integrated wind stress. The area under each graph represents the volume of water entrained at the coast during the scenario. The first scenario consists of a wind event of a particular strength and duration. The second scenario, however, consists of a wind event of half the stress of the event in the first scenario, but which blows for twice as long. Examination of the area underneath the graphs, indicates that the same volume of water is entrained in the two scenarios. This implies that entrainment depends linearly on the wind stress, although it must be remembered that the wind stress does not depend linearly on the wind speed. The third scenario consists of two separate wind events, which both blow at the same speed as the wind event in the second scenario, but which only blow for half as long. It can clearly be seen that the volume of water entrained in this third scenario is significantly less than the volume entrained in the first two scenarios. This is due to the time delay between the onset of the wind stress and the commencement of entrainment. The third scenario contains two of these time delays, because it consists of two separate events, while the other scenarios each only contain one time delay. This result implies that frequent wind events of a short duration entrain less water than longer wind events, even if they have the same cumulative wind stress. Because the time delay that causes this difference in entrainment is a function of the wind stress, the difference between the entrainment that occurs in the two scenarios will also be a function of the wind stress. Using the cumulative wind stress in order to approximate the entrainment occuring over several wind events will, therefore, be more accurate for large values of the cumulative wind stress than for small values. This point needs to be remembered if a seasonal cumulative wind stress is used in an attempt to determine the quantity of water entrained over a seasonal time scale.

4.3 Results of simple budgets

The effect of the strength of the wind event on the nutrient and heat budgets at the coast can be assessed with the assistance of figure 4.10. This figure illustrates the offshore variation in the entrainment length at $t_* = 6\pi$ (approximately three days), for the strong, fresh and moderate wind events of the previous section. The offshore scale extends from the coast to a point two baroclinic radii offshore. In Saldanha Bay, however, the interest is in the entrainment that occurs immediately adjacent to the coast and, particularly, within one baroclinic radius of the coast. Horizontal advection and mixing in this coastal zone is likely to ensure that mean budgets for the coastal zone are more realistic than budgets evaluated at particular points. The area underneath each graph, between $y_* = 0$ and $y_* = 1$, represents the quantity of water entrained within one radius of the coast, per unit length of coastline. Estimates of this quantity of water will now be used to determine the mean nutrient and heat budgets within the coastal zone (within one radius of the coast). Within this area, the mean entrainment length after three days for the various events is approximately:

- strong event: entrainment length $\simeq 3.2$

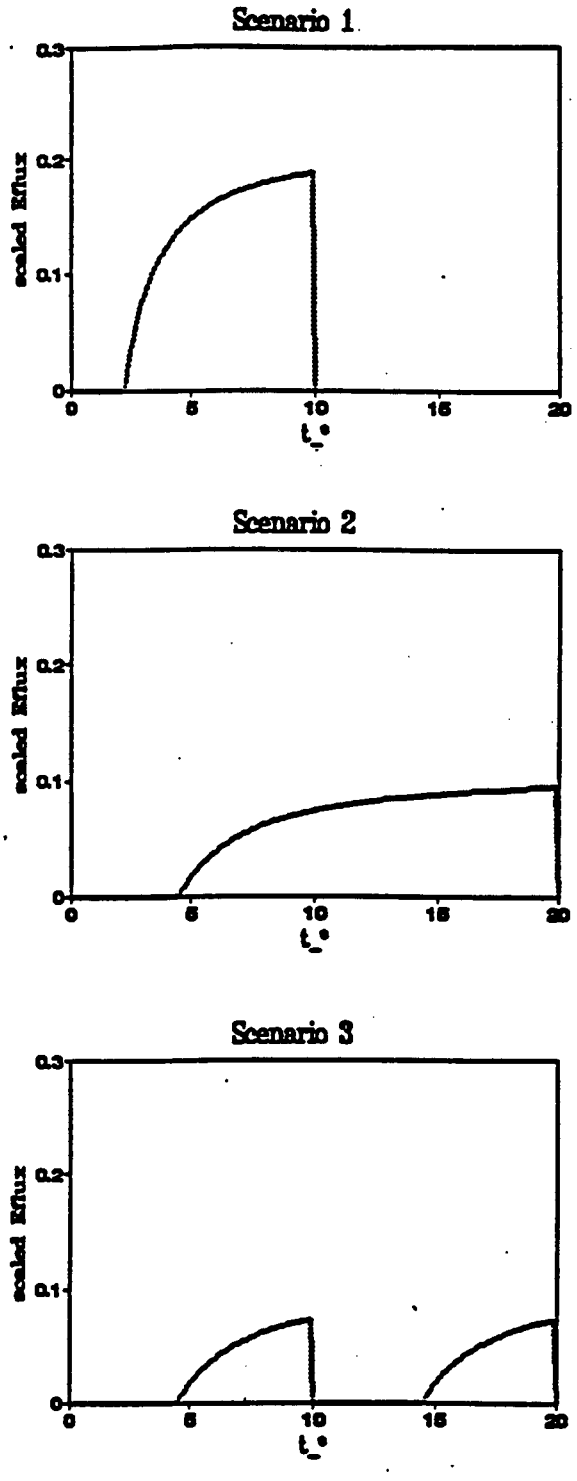

Figure 4.9: Graph showing the variation of the scaled entrainment flux with time for three different scenarios. The first scenario consists of a single wind event, which blows at $X_s = 0.2$ for $t_* = 10$. The second scenario also consists of a single wind event, but this wind event blows at $X_s = 0.1$ for $t_* = 20$. The third scenario consists of two separate wind events, which each blow at $X_s = 0.1$ for $t_* = 10$. All three scenarios have the same time-integrated wind stress.

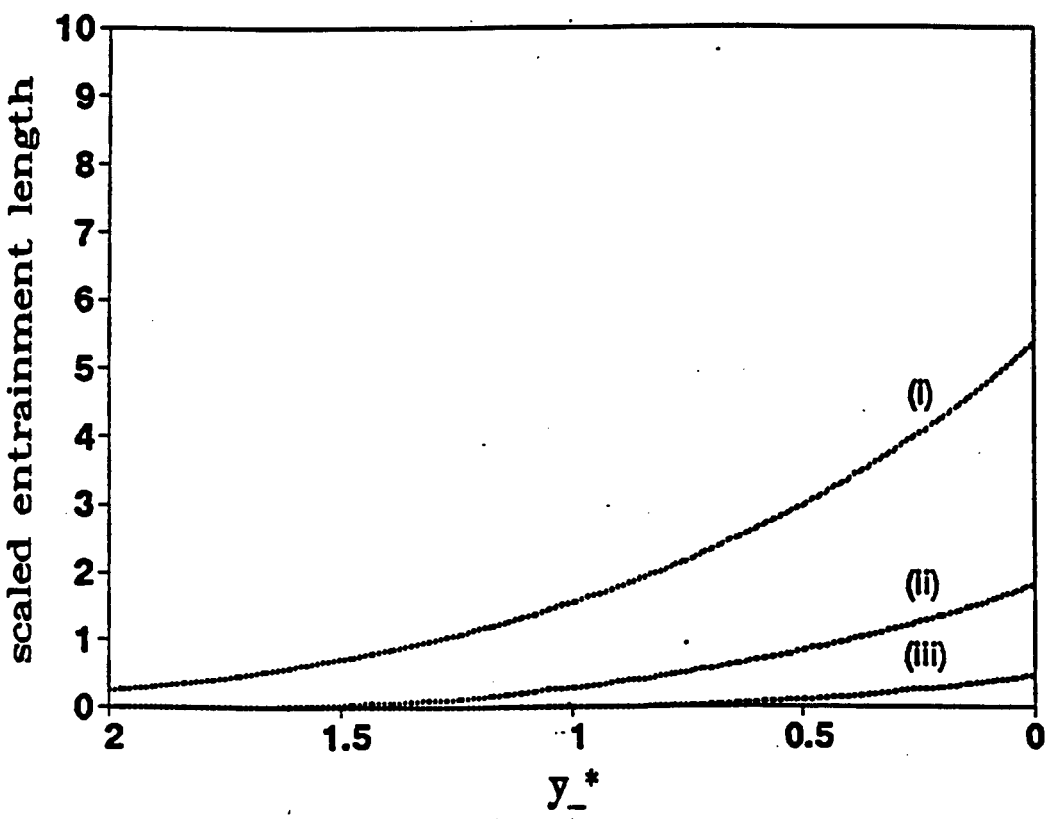

Figure 4.10: Graph depicting the variation in the scaled entrainment length with offshore distance (at $t_* = 6\pi$) for a wind event of (i) $13.4m.s^{-1}$, (ii) $9.3m.s^{-1}$, and (iii) $6.2m.s^{-1}$. The respective values of F are 0.213, 0.038 and 0.008.

- fresh event: entrainment length $\simeq 0.9$
- moderate event: entrainment length $\simeq 0.1$

This entrainment length is scaled against the initial upper layer depth (h_1). Multiplying by $h_1 = 15m$, will give the mean volume of water that has been entrained, per square metre. The mean volume flux ($Eflux$), within one radius of the coast, can then be obtained by dividing the volume by the duration of the wind event:

- strong event: $Eflux \simeq 2.0 \times 10^{-4} m^3.s^{-1}.m^{-2}$
- fresh event: $Eflux \simeq 5.7 \times 10^{-5} m^3.s^{-1}.m^{-2}$
- moderate event: $Eflux \simeq 6.3 \times 10^{-6} m^3.s^{-1}.m^{-2}$

These average volume fluxes illustrate the sensitivity of the quantity of water entrained in an event, to the intensity of the wind event. The average volume fluxes can be converted into fluxes of nutrient and heat from the lower layer to the upper layer. If the assumption is made that $[NO_3] = 20mM.m^{-3}$ in the lower layer (see chapter 2), and negligible in the upper layer, then the mean nitrate flux, per hour, is given by:

- strong event: nitrate flux $\simeq 14mM.hour^{-1}.m^{-2}$
- fresh event: nitrate flux $\simeq 4mM.hour^{-1}.m^{-2}$
- moderate event: nitrate flux $\simeq 0.5mM.hour^{-1}.m^{-2}$

The simple nutrient budget, presented in the previous chapter, showed that this mean influx of nitrate is approximately equal to the mean nitrate uptake rate during the wind event. In reality, these values represent the maximum possible uptake rates, because a significant percentage of the nitrate uptake will occur after the wind has subsided.

The estimates of the mean volume flux from the lower layer into the upper layer, within the coastal zone, can also provide information about the heat budget. For ease of reference, the simple heat budget presented in the previous chapter (see equation 3.56) can be rewritten:

$$Cp.\rho.H_1(t).\frac{dT_1}{dt} = Cp.\rho.Eflux.[T_2 - T_1(t)] + Q \qquad (4.3)$$

Each term in this equation has units $W.m^{-2}$. Initially, the upper layer temperature is fixed. The density difference, that was assumed in the previous section, between the two layers is approximately equivalent to a temperature difference of $8°C$. Given the mean entrainment flux adjacent to the coast, the flux of heat due to entrainment can be calculated for the initial stratification situation. The results for the various wind events are:

- strong event: $Cp.\rho.Eflux.[T_2 - T_1(t)] \simeq -6848W.m^{-2}$

- fresh event: $Cp.\rho.Eflux.[T_2 - T_1(t)] \simeq -1952W.m^{-2}$
- moderate event: $Cp.\rho.Eflux.[T_2 - T_1(t)] \simeq -216W.m^{-2}$

The daily average surface heat flux in the vicinity of Saldanha Bay in summer can approach values of $Q \simeq 340W.m^{-2}$ (see Guastella 1992). This suggests that the temperature of the upper layer will increase, during moderate wind events, because the input of heat through the water surface is likely to be greater than the cooling due to the entrainment of cold water. However, for fresh and strong wind events, the upper layer must cool, because the cooling due to entrainment is greater than the heating due to the surface heat flux. There will be a particular strength of wind event for which entrainment exactly balances the surface heat flux, and the upper layer temperature remains constant.

As long as the cooling due to entrainment is larger than the surface heat flux, the temperature of the upper layer will decrease. This will reduce the cooling effect of entrainment. Eventually the upper layer will be cooled to a temperature that results in a balance between the surface heat flux and entrainment. A similar argument applies for the situation where the surface heat flux is larger than entrainment. Given a surface heat flux of $340W.m^{-2}$, the temperature difference that is eventually approached is:

- strong event: $T_1 - T_2 \simeq 0.4°C$
- fresh event: $T_1 - T_2 \simeq 1.4°C$
- moderate event: $T_1 - T_2 \simeq 12.6°C$

The temperature difference between the two layers will clearly change dramatically from the initial $8°C$, due to surface heating and entrainment. It needs to be stressed, however, that the values of $Eflux$ have been determined by assuming that the density difference between the two layers remains constant. If the temperature change occurs over a time scale that is comparable to the typical duration of an upwelling event, then the assumption of a constant density difference between the layers will be invalid. The feedback between entrainment and stratification has been neglected in the model of coastal entrainment.

Work by Monteiro and Brundrit (in press) has shown that in midsummer the temperature of the upper layer of Saldanha Bay decreases by at most $2°C$ during a wind event. If this event lasts for three days, and if the mean depth of the upper layer during this event is $10m$, then the cooling of the upper layer would require a net heat flux loss of roughly:

$$Cp.\rho.H_1(t).\frac{dT_1}{dt} \simeq 4180 \times 1024 \times 10 \times \frac{-2}{86400 \times 3} \quad (4.4)$$

$$\simeq -330W.m^{-2} \quad (4.5)$$

If a value of $340W.m^{-2}$ is assumed for the surface heat flux, the flux of heat due to entrainment must be:

$$Cp.\rho.Eflux.[T_2 - T_1(t)] \simeq -340W.m^{-2} - 330W.m^{-2} \quad (4.6)$$

$$\simeq -670W.m^{-2} \quad (4.7)$$

If the mean temperature difference between the layers during the entrainment event is $7°C$:

$$Eflux \simeq 2 \times 10^{-5} m^3.s^{-1}.m^{-2} \quad (4.8)$$

The entrainment flux that is required to cool the upper layer by $2°C$ in three days is an order of magnitude smaller than the entrainment flux expected from a strong wind event. An entrainment flux of $2 \times 10^{-5} m^3.s^{-1}.m^{-2}$ is in fact consistent with a moderate to fresh wind event. A strong wind event should thus cool the upper layer of Saldanha Bay by significantly more than $2°C$. The observed upper layer cooling suggests that the morphology of Saldanha Bay modifies the heat budget from the situation that is applicable along a straight coastline. This point will be amplified, in the following chapter.

4.4 Summary

This chapter has presented some of the results of the model of coastal entrainment introduced in the previous chapter. Three stages can be identified in a typical entrainment event. The first stage consists of the establishment of offshore and longshore shear, and linear upwelling of the interface. No entrainment takes place. Entrainment begins in the second stage, and rapidly reduces the rate of interfacial upwelling to a level where the upwelling flux is all but negligible. The third stage commences when this upwelling rate has become negligible. In this stage, the position of the interface is approximately constant, and the flux of water entrained into the upper layer is steady. The entrainment is fully realised. The duration of these various stages depends on the offshore position, and on the strength of the wind event (that is on F).

The results presented in this chapter show that entrainment is most vigorous at the coast, and that it decreases in a near-exponential fashion away from the coast for large times. This result implies that the flux of nutrients into the upper layer, and thus the uptake rate of nutrients in the upper layer, will decrease near-exponentially away from the coast. The offshore variation in entrainment will also influence the heat budget by injecting greater quantities of colder water into the upper layer at the coast than further offshore. The cooling effect of entrainment on the heat budget will thus be most pronounced at the coast. The slope of the interface, meanwhile, is altered by entrainment from an exponential shape during the first stage, to a near-linear slope during the third stage. This interfacial slope is small compared to the slope before entrainment begins, and is indicative of how entrainment reduces the longshore shear in the model. The inter-

face never reaches the surface of the water, ensuring that there are always two layers in the system.

Comparison of the effects of different wind events on entrainment showed that entrainment is sensitive to the intensity of the wind event. Significantly more entrainment occurs in strong wind events than in weaker events, which is not surprising. What is surprising, however, is that the interface position in stage three is remarkably insensitive to the strength of the wind event. This means that the interface position should not be used as a diagnostic for the entrainment that has occured. The results also showed that strong wind events will be associated with surface mixed layers that are marginally shallower than for weaker wind events. This finding is opposite to the situation in the open ocean. Comparison of the entrainment occuring during particular scenarios that have the same cumulative wind stress indicates that an identical amount of entrainment occurs in the scenarios if they each consist of only one event. If, however, one of the scenarios consists of two or more separate wind events, the time delay between the beginning of the wind event and the commencement of entrainment will result in less water being entrained into the upper layer in this scenario. The difference in the quantity of water entrained between the scenarios will be a function of wind stress.

The average nutrient and heat budgets for the ocean within a baroclinic radius of the coast were investigated for the strong, fresh and moderate wind events. As would be expected, the nutrient flux into the upper layer is significantly greater during strong wind events than during weak events. The simple heat budget indicated that the temperature of the upper layer would decrease during strong and fresh wind events, but that the temperature would increase during moderate wind events. Work by Monteiro and Brundrit (in press) indicates that the upper layer of Saldanha Bay cools by approximately $2°C$ during the strongest wind events. A simple calculation shows, however, that the entrainment that would result in a cooling of $2°C$ corresponds to a moderate to fresh wind event. A large wind event should, therefore, result in a significantly greater temperature drop. The morphology of the bay must in some way alter the heat budget, so as to prevent the upper layer temperature from decreasing to the same extent as it would along an open coastline.

Chapter 5

DISCUSSION

5.1 Coastal entrainment

The main objective of this thesis was to quantify the amount of water that is entrained by the upper layer of Saldanha Bay from the lower layer. A survey of the available literature suggested that the bay is isothermal in winter, but that it separates into two vertical layers during summer. The upper layer is warm and nutrient-depleted, while the lower layer is cold and nutrient-rich. The appearance of the cold bottom layer in the bay appears to be in response to the upwelling favourable winds which drive the large-scale coastal upwelling that characterizes the Benguela system. Because entrainment cannot occur when the bay is isothermal, the study focuses on the summer months.

Entrainment of water across an interface occurs if the velocity shear across the interface overcomes the stabilising effects of stratification. This can be represented by a Richardson number argument, where entrainment commences when the Richardson number reduces to a critical value. The entrainment deepens the position of the interface, which increases the stratification, and thus reduces the Richardson number. There is a feedback between the Richardson number and entrainment. Once the Richardson number has become critical, entrainment proceeds at a rate that ensures that the Richardson number never becomes subcritical (Pollard et al 1973). In the open ocean, the surface mixed layer is most likely to entrain water from below at the beginning of winter. In these circumstances the winter loss of heat to the atmosphere reduces the stratification to such an extent that large wind events can cause critical Richardson numbers and entrainment. The large positive surface heat flux in the Benguela region during spring and summer will increase the stratification of the water column. This means that subsequent summer wind events are unlikely to result in entrainment far offshore. Closer to the coast, however, the coastal upwelling that is associated with the summer wind events, alters both the stratification and the velocity shear terms from their open ocean values. In order to investigate shear driven entrainment during coastal upwelling events, a simple two layer model of coastal upwelling was

introduced. Quasi-steady solutions to this upwelling model were used, because it was established that inertial oscillations normally decay to negligible levels by the time that entrainment begins. The additional assumption was made that entrainment does not affect the density of the upper layer. This important assumption was made to ensure that entrainment does not alter the upper layer divergence in the model. Unfortunately the entrainment process tends to reduce the long-shore shear across the interface in the model, which prevents an analytical solution from being obtained. Instead, minimum and maximum constraints on the quantity of entrainment that takes place were investigated. These constraints can be numerically determined so as to provide an approximation to the amount of entrainment that occurs in a given scenario. A model of coastal entrainment has thus been presented, which seeks to quantify the amount of entrainment that occurs along an open coast. Limitations regarding the validity of the model, and its applicability to Saldanha Bay, will be discussed in the paragraphs that follow.

A secondary objective of this thesis was to determine simple nutrient and heat budgets for the upper layer of Saldanha Bay. These budgets depend critically on the flux of cold nutrient-rich water entrained from the lower layer into the upper layer. The model of coastal entrainment was thus used to provide the flux of entrained water required in the simple budgets.

Several approximations were made in the model to keep the entrainment problem as simple as possible. These approximations will, however, mean that there will be some difference between the model of entrainment presented, and the actual entrainment occuring in a bay such as Saldanha. The first approximation that will be considered is that the wind stress is constant. This can obviously only be approximately true for short periods. A time varying wind stress will clearly change the time at which entrainment begins, and the quantity of water entrained. The really interesting case, however, arises when a component of the wind stress fluctuates at the same frequency as the coriolis parameter. Chapter 3 demonstrated that inertial oscillations are relatively unimportant in the coastal entrainment process, because these oscillations have decayed to insignificant levels by the time that entrainment begins. A time varying wind stress, however, may establish resonant inertial oscillations that are significant when entrainment begins. The presence of inertial oscillations in the depth of the interface will impact on the time that it takes the Richardson number to become critical, and may also cause entrainment to be pulsed, as in the model of Pollard et al (1973). The oscillations in the velocity shear, meanwhile, will cause the shear to be larger than when the oscillations are absent. This will cause the Richardson number to become critical sooner, and may also result in pulsed entrainment. Oscillations that increase in amplitude with time, rather than decaying, may eventually result in the upper layer entraining the entire lower layer, and extending to the bottom of the sea. As was indicated in chapter 2, Saldanha Bay lies at a latitude where the diurnal frequency of land-sea breezes is close to that of the coriolis parameter, making resonant inertial oscillations a possibility. The effect of the coastal boundary on resonant inertial oscillations needs to be investigated.

Another approximation that has been made is that the momentum from the wind is imparted into a layer of constant thickness h_1 (see chapter 2). In reality, however, upwelling of the interface causes the momentum to be imparted into a thinning layer. This will cause the shear terms and the interface displacement to increase more rapidly than is indicated by the model. The Richardson number will become critical sooner, and entrainment will proceed towards solely satisfying the upper layer divergence more rapidly than is indicated by the model. The model will, therefore, underestimate the amount of entrainment occuring during a wind event.

A crucial component of the entrainment model is the assumption that the upper layer density does not change significantly during a wind event. This approximation would be valid if the surface heat flux was balanced by the entrainment of cold water from the lower layer. The previous chapter suggested, however, that for strong and fresh wind events the entrainment of cold water would dominate the surface heat flux in the coastal zone. This will cause the upper layer to cool during a wind event. Therefore, as entrainment proceeds, the density difference between the two layers will be reduced. The reduction in stratification should enhance entrainment, but this may be partially offset by reductions in the offshore and longshore velocity shears. If entrainment is enhanced by a feedback loop, the entrainment flux will not be limited to merely satisfying the upper layer divergence. Instead, entrainment may force the interface down below its original level. The interface separating the two layers will not reach the surface, but the cooling of the upper layer, driven by the entrainment, will represent a horizontal entrainment front. This feedback loop is ignored in the model of coastal entrainment that has been presented. Along an open coast, the results of the previous chapter indicate that it would be difficult to justify ignoring the change in upper layer temperature during a wind event. The model of coastal entrainment is thus not really valid along an open coast. In Saldanha Bay, however, the strongest wind events appear to cool the upper layer by only $2°C$ (Monteiro and Brundrit, in press). This relatively small change in the upper layer temperature means that the coastal entrainment model can be applied to Saldanha Bay without introducing unacceptable error.

The seasonal signal in stratification in Saldanha Bay will be determined by a succession of synoptic events. During quiescent phases of the synoptic cycle, the upper layer will warm under the influence of the surface heat flux. Strong wind events, however, will result in entrainment and cooling of the upper layer. The cumulative effect of these warming and cooling periods determines the seasonal pattern of the upper layer temperature. During the initial stages of the upwelling season, the temperature difference between the upper and lower layers is small, so that entrainment events have a small cooling effect on the upper layer. Helped by the increasing surface heat flux during these initial stages of the upwelling season, the upper layer is allowed to warm to its seasonal maximum. During the latter stages of the upwelling season, this process is reversed, and the decreasing surface heat flux helps entrainment events to cool the upper layer.

The seasonal cycle of stratification in Saldanha Bay can be viewed in Monteiro and Brundrit (in press) for the austral summer of 1993/1994. During the approximately three month period from early to mid-summer, the temperature difference between the upper and lower layers increased from $6°C$ to $10°C$. Because the temperature of the lower layer remains fairly constant, this implies that the upper layer warms by $4°C$ over the three month period. If the mean depth of the upper layer is $10m$ over this period, then the mean net heat flux required to achieve this warming will be:

$$Cp.\rho.H_1(t).\frac{dT_1}{dt} \simeq 4180 \times 1024 \times 10 \times \frac{4}{86400 \times 90} \tag{5.1}$$

$$\simeq 22W.m^{-2} \tag{5.2}$$

This result suggests that the mean surface heat flux over the three month period is approximately $22W.m^{-2}$ greater than the mean entrainment heat flux over the same period. Chapter 2 indicated that there is approximately a six day periodicity in upwelling-favourable winds over the Benguela. The assumption will thus be made that the average wind event lasts for three days, and that it is followed by three days of calm conditions. If the assumption is also made that the average wind event over the three month period corresponds to a fresh wind event, and that the mean temperature difference between the layers over the same period is $8°C$, then the entrainment heat flux will be approximately:

$$Cp.\rho.Eflux.[T_2 - T_1(t)] \simeq -5.7 \times 10^{-5} \times 4180 \times 1024 \times 8 \times \frac{1}{2} \tag{5.3}$$

$$\simeq -976W.m^{-2} \tag{5.4}$$

Over the three month period, Guastella (1992) indicates that the mean surface heat flux is likely to be of the order of:

$$Q \simeq 250W.m^{-2} \tag{5.5}$$

The mean surface heat flux over the three month period is thus much smaller than the corresponding mean entrainment heat flux. This crude calculation indicates that the upper layer of the bay should cool over the three months, rather than warm.

The observed seasonal warming of the bay can be explained if the heat budget is altered by the morphology of the bay. The model of entrainment, and the upper layer budgets, were derived for a straight coastline. Saldanha Bay, however, is only connected to the open ocean via a comparatively narrow channel. The width of this channel is probably the appropriate length scale of coast over which entrainment occurs. Surface heating, however, operates over the entire surface area of the bay. Examination of a map of Saldanha Bay (see figure 1.1), shows that the width of the channel is approximately $4000m$. The length scale perpendicular to the axis of the channel is approximately $8000m$. This suggests that the entrainment flux in Saldanha Bay is operating over an effective area of some $32 \times 10^6 m^2$. The actual surface area of the Saldanha Bay

system is, however, approximately $135 \times 10^6 m^2$ (Shannon and Stander 1977). Within the bay, therefore, the mean entrainment heat flux is:

$$Cp.\rho.Eflux.[T_2 - T_1(t)] \simeq -976 \times \frac{32 \times 10^6}{135 \times 10^6} \quad (5.6)$$

$$\simeq -231 W.m^{-2} \quad (5.7)$$

The mean surface heat flux is thus of the order of $19 W.m^{-2}$ greater than the entrainment heat flux over the same period. This is comparable to the net heat flux required to produce the observed seasonal warming. This rather suggestive result would appear to indicate that the morphology of the bay alters the heat budget of Saldanha Bay, preventing the upper layer from cooling dramatically during entrainment events. The morphology of the bay thus allows the feedback loop between entrainment and stratification to be ignored.

The morphology of Saldanha Bay not only alters the heat budget from that of an open coast, but will also alter the nutrient budget. Because the effective area over which entrainment occurs in Saldanha Bay appears to be approximately $32 \times 10^6 m^2$, the nutrient fluxes presented in the previous chapter can be modified to take the morphology of the bay into account. The adjusted nutrient fluxes will be:

- strong event: nitrate flux $\simeq 14 \times \frac{32 \times 10^6}{135 \times 10^6} \simeq 3 mM.hour^{-1}.m^{-2}$
- fresh event: nitrate flux $\simeq 4 \times \frac{32 \times 10^6}{135 \times 10^6} \simeq 1 mM.hour^{-1}.m^{-2}$
- moderate event: nitrate flux $\simeq 0.5 \times \frac{32 \times 10^6}{135 \times 10^6} \simeq 0.1 mM.hour^{-1}.m^{-2}$

These are the mean nitrate fluxes, and thus nitrate uptake rates, that the model predicts for Saldanha Bay during the wind events.

5.2 New knowledge

The main work of this thesis has been to attempt to produce a model of the entrainment that occurs during a coastal upwelling event. The previous section has shown that the morphology of the bay enables a simplification to be made in the derivation of this model. Along an open coastline, this simplification cannot be made, and the model that has been presented is invalid. The model is thus only likely to be relevant in semi-enclosed bays, large estuaries, and very large harbours, where there can be an approximate balance between the surface heat flux and the heat flux due to entrainment. The model is also limited to areas of very strong stratification, because it assumes that the system is two layered.

Three stages can be identified during an upwelling-favourable wind event. In the first stage, the interface separating the two layers upwells linearly with time, and no entrainment occurs. The

second stage commences when entrainment begins, and this entrainment flux causes a reduction in the rate at which the interface upwells. In the third stage entrainment is fully realised, and the position of the interface is approximately steady. During this third stage, the entrainment flux fully satisfies the upper layer divergence. Entrainment is thus most vigorous at the coast, and decreases away from the coast in a near-exponential fashion. The position of the interface, however, decreases linearly away from the coast. An important finding is that the final position of the interface is remarkably insensitive to the strength of the wind event, which implies that the position of the interface is a poor diagnostic for entrainment. The results presented in the previous section for strong, fresh and moderate wind events, suggest that the steady position of the interface in the model is approximately 25% of the initial upper layer depth. The observed depth of the thermocline that separates the two layers in the bay is likely to represent this steady interface position. The model suggests that strong wind events will result in marginally shallower thermoclines within the bay than are evident for weak wind events. This is opposite to the situation in the absence of coastal influences. The depth of this thermocline should increase linearly away from the coast.

By quantifying entrainment in the bay, the model provides an indication of the flux of nutrients into the upper layer of Saldanha Bay. Examination of the heat budget indicates that the appropriate length scale for entrainment in Saldanha Bay is the width of the channel linking the bay to the open ocean. The appropriate area over which to calculate the nutrient flux into the upper layer of the bay appears to be of the order of $32 \times 10^6 m^2$. This is less than a quarter of the area of the Saldanha Bay system. The nutrient flux decreases in a near-exponential fashion away from the coast, and is highly sensitive to the strength of the wind event. These estimates of the nutrient flux, and the nutrient uptake rate, are important for the effective management of water quality in Saldanha Bay. Hopefully the model presented in this thesis could be used to provide management information in similar systems worldwide.

The results have also shown that the same quantity of water, and thus nutrient, will be entrained in events that have the same cumulative wind stress. However, less water will be entrained in a scenario that consists of several separate wind events than in a scenario consisting of one event, even if the scenarios have the same cumulative wind stress. Less entrainment will thus occur during seasons when the upwelling favourable winds are frequently pulsed, than in seasons when the winds are steadier. This provides a link between interannual variability in the frequency of wind events and the nutrient flux into the upper layer of Saldanha Bay.

5.3 Future research

The model needs to be validated in order to determine its usefulness to the management of Saldanha Bay. Validation of the model can occur in several ways. Firstly, the offshore variation of

the thermocline in the bay can be investigated. If the depth of the thermocline increases linearly away from the coast, some supporting evidence for the model will have been found. Nitrate uptake rates within the bay can also be investigated to establish the validity of the budget estimates. The nutrient and heat budgets are both highly dependent on the same process, that is entrainment. Comparison of nitrate uptake rates with temperature information from the bay, can thus give information about the entrainment process. This knowledge might be used to provide more accurate estimates of the effective area over which entrainment occurs in Saldanha Bay.

Extension of the model to include effects that have been neglected is possible. An important advance would be to incorporate a time-varying wind stress. The particularly interesting possibility of resonant inertial oscillations could then be included in the entrainment dynamics of Saldanha Bay. Perhaps the most important extension to the model would be to allow the density of the upper layer to vary. This would convert the constant F into a variable. Allowing the feedback loop between entrainment and stratification would extend the validity of the model to all upwelling coastlines.

REFERENCES

ANDERSON, D.L.T. and GILL, A.E. (1979)
Beta dispersion of inertial waves.
Journal of Geophysical Research, Vol. 84, 1836-1842.

ANDERSON, I., HUYER, A. and SMITH, R.L. (1983)
Near-inertial motions off the Oregon coast.
Journal of Geophysical Research, Vol. 88, 5960-5972.

BAINES, P.G. (1986)
Internal tides, internal waves, and near-inertial motions.
in Baroclinic Processes on Continental Shelves
Coastal and Estuarine Sciences, Vol. 3, ed. Mooers, American Geophysical Union, Washington, 19-31.

BOYD, A.J. (1981)
An intensive study of the currents and general hydrology of an anomalous upwelling area off South West Africa.
MSc Thesis, University of Cape Town, 170pp.

CSIR **a** (1976)
Saldanha Bay. Feasability study and recommended approach for the modelling of Saldanha Bay and Langebaan Lagoon.
Rep.S.Afr.Coun.scient.ind.Res. C/SEA 7620/1, 24pp. + tables, charts and appendices.

CSIR **b** (1976)
Saldanha Bay. The assesment of field data, the mathematical model and the physical model.
Rep.S.Afr.Coun.scient.ind.Res. C/SEA 7620/2, unnumbered.

D'ADAMO, N., SIMPSON, C., MILLS, D., IMBERGER, J. and MCCOMB, A. (1992)
The influence of stratification on the ecological response of two Western Australian embayments to nutrient enrichment.
in Marine Coastal Eutrophication, ed. Vollenwieder, Marchetti and Viviani, Elsevier, Amsterdam, 829-850.

GILL, A.E. (1982)
Atmosphere-Ocean Dynamics.
International Geophysics Series, Vol. 30, ed. Donn, Academic Press, London, 662pp.

GUASTELLA, L.A-M. (1992)
Sea surface heat exchange at St Helena Bay and implications for the Southern Benguela Upwelling System.
S.Afr.J.mar.Sci., Vol. 12, 61-70.

HALPERN, D. (1974)
Observations of the deepening of the wind mixed layer in the Northeast Pacific Ocean.
Journal of Physical Oceanography, Vol. 4, 454-466.

KRAUSS, W. (1981)
The erosion of a thermocline.
Journal of Physical Oceanography, Vol. 11, 415-433.

LARGE, W.G. and POND, S. (1981)
Open ocean momentum flux measurements in moderate to strong winds.
Journal of Physical Oceanography, Vol. 11, 324-336.

LARGIER, J.L. (1990)
Deep surface mixed layers on the continental shelf.
Continental Shelf Research, Vol. 10, 759-776.

LENTZ, S.J. (1992)
The surface boundary layer in coastal upwelling regions.
Journal of Physical Oceanography, Vol. 22, 1517-1539.

MILLOT, C. and CREPON, M. (1981)
Inertial oscillations on the continental shelf of the Gulf of Lions - observations and theory.

Journal of Physical Oceanography, Vol. 11, 639-657.

MONTEIRO, P.M.S. and BRUNDRIT, G.B. (1990)
Interannual chlorophyll variability in South Africa's Saldanha Bay system, 1974-1979.
S.Afr.J.mar.Sci., Vol. 9, 281-287.

MONTEIRO, P.M.S. and BRUNDRIT, G.B. (1995)
Shelf-Bay interactions in the southern Benguela upwelling system: implications for eutrophication.
submitted to Estuarine and Coastal Shelf Science.

POLLARD, R.T. (1970)
On the generation by winds of inertial waves in the ocean.
Deep-Sea Research, Vol. 17, 795-812.

POLLARD, R.T. and MILLARD, R.C.JR. (1970)
Comparison between observed and simulated wind-generated inertial oscillations.
Deep-Sea Research, Vol. 17, 813-821.

POLLARD, R.T., RHINES, P.B. and THOMPSON, R.O.R.Y. (1973)
The deepening of the wind-mixed layer.
Geophys.Fluid Dyn., Vol. 4, 381-404.

PRESTON-WHYTE, R.A. and TYSON, P.D. (1988)
The Atmosphere and Weather of Southern Africa., Oxford University Press, Cape Town, 374pp.

SHANNON, L.V. (1985)
The Benguela ecosystem part 1: Evolution of the Benguela, physical features and processes.
Oceanography and Marine Biology Annual Review, Vol. 23, 105-182.

SHANNON, L.V. and STANDER, G.H. (1977)
Physical and chemical characteristics of water in Saldanha Bay and Langebaan Lagoon.
Trans.Roy.Soc.S.Afr., Vol. 42, 441-459.

WEEKS, S.J., BOYD, A.J., MONTEIRO, P.M.S. and BRUNDRIT, G.B. (1991)
The currents and circulation in Saldanha Bay after 1975 deduced from historical measurements of drogues.
S.Afr.J.mar.Sci., Vol. 11, 525-535.

WEEKS, S.J., MONTEIRO, P.M.S., NELSON, G. and COOPER, R.M. (1991)
A note on wind-driven replacement flow of the bottom layer in Saldanha Bay, South Africa: implications for pollution.
S.Afr.J.mar.Sci., Vol. 11, 579-583.